

Closed orbits and spatial density oscillations in the circular billiard

Matthias Brack and Jérôme Roccia

Institute for Theoretical Physics, University of Regensburg, D-93040 Regensburg,
Germany

Abstract. We present a case study for the semiclassical calculation of the oscillations in the particle and kinetic-energy densities for the two-dimensional circular billiard. For this system, we can give a complete classification of all closed periodic and non-periodic orbits. We discuss their bifurcations under variation of the starting point r and derive analytical expressions for their properties such as actions, stability determinants, momentum mismatches and Morse indices. We present semiclassical calculations of the spatial density oscillations using a recently developed closed-orbit theory [Roccia J and Brack M 2008 *Phys. Rev. Lett.* **100** 200408], employing standard uniform approximations from perturbation and bifurcation theory, and test the convergence of the closed-orbit sum.

PACS numbers: 03.65.Sq, 03.75.Ss, 05.30.Fk, 71.10.-w

1. Introduction

We have recently developed [1, 2] a semiclassical theory, based on Gutzwiller's semiclassical approximation of the single-particle Green function [3], for spatial density oscillations in quantum systems consisting of N non-interacting fermions bound in a local mean-field potential $V(\mathbf{r})$. While the average parts of the particle and kinetic-energy densities are given by the extended Thomas-Fermi theory (see, e.g., [4], chapter 4), their oscillating parts could be expressed [1] as sums over all closed, in general non-periodic orbits of the corresponding classical system, starting and ending at the same space point \mathbf{r} . The semiclassical evaluation of the spatial density oscillations requires the knowledge of all closed non-periodic orbits and their actions, stability determinants, momentum mismatches and Morse indices (as specified in the next section), which in general can only be determined numerically. The resulting formulae are the analogues of the semiclassical trace formulae for the level density, initiated by Gutzwiller [3], in terms of periodic orbits.

As an outcome of the semiclassical theory, some "local virial theorems" connecting kinetic and potential energy densities at any given point \mathbf{r} and some (integro-) differential equations for the particle density $\rho(\mathbf{r})$, that previously had been proved to hold exactly for isotropic harmonic oscillators with closed shells [5] and for linear potentials [2] in D spatial dimensions, could be generalized to arbitrary local potentials. Formally, they hold in general only in the semiclassical limit $\hbar \rightarrow 0$, corresponding to $N \rightarrow \infty$, but in various model potentials they have been shown [2] to be well fulfilled even for moderate particle numbers N .

The present paper is a case study for the two-dimensional circular billiard, for which we can classify all closed orbits and determine their properties analytically, and that allows us to study the convergence of the orbit sum in the semiclassical formulae for the spatial density oscillations. In section 2 we summarize the main results of the semiclassical theory. In section 3 we investigate the closed orbits of the circular billiard. We give a complete classification of all periodic and non-periodic orbits, including their bifurcations that can occur at specific distances r_b from the center, and present analytical expressions for their properties required in the semiclassical theory. In section 4 we discuss the regularizations that become necessary at critical points where the semiclassical amplitudes diverge for different reasons. These are the center $r = 0$ (symmetry breaking), the bifurcation points r_b ($0 < r_b < R$), and the boundary $r = R$ (zero length of the shortest orbit). In section 5 we present results for the spatial density oscillations and test, in particular, their convergence and its relation to the shell effects in the total energy. In the appendix, we give explicit analytical results for the properties of some of the shortest orbits.

2. Semiclassical closed-orbit theory

In this section we present the general framework and the main results of the semiclassical theory for spatial density oscillations developed in [1, 2]. We consider a D -dimensional system of N non-interacting particles with mass m , obeying Fermi-Dirac statistics and bound by a local potential $V(\mathbf{r})$. $V(\mathbf{r})$ may represent the self-consistent local mean field of an *interacting* fermion system, such as it is obtained in density functional theory, or just a given model potential. The discrete energy eigenvalues E_j and eigenfunctions $\psi_j(\mathbf{r})$ are given by the stationary Schrödinger equation. The quantum-mechanical particle density of the system at zero temperature, including a factor two for the spin degeneracy, is given by

$$\rho(\mathbf{r}) = 2 \sum_{E_j \leq \lambda} \psi_j^*(\mathbf{r}) \psi_j(\mathbf{r}), \quad \int \rho(\mathbf{r}) d^D r = N, \quad (1)$$

where the Fermi energy $\lambda = \lambda(N)$ is determined by the normalization of the density to the given particle number N (which is here taken as an even integer). For the kinetic-energy density we discuss two different forms

$$\tau(\mathbf{r}) = -\frac{\hbar^2}{2m} 2 \sum_{E_j \leq \lambda} \psi_j^*(\mathbf{r}) \nabla^2 \psi_j(\mathbf{r}), \quad (2)$$

$$\tau_1(\mathbf{r}) = \frac{\hbar^2}{2m} 2 \sum_{E_j \leq \lambda} |\nabla \psi_j(\mathbf{r})|^2, \quad (3)$$

which upon integration both lead to the exact total kinetic energy. We also investigate the average of these two kinetic-energy densities:

$$\xi(\mathbf{r}) = \frac{1}{2} [\tau(\mathbf{r}) + \tau_1(\mathbf{r})]. \quad (4)$$

Due to the assumed time reversal symmetry and spin degeneracy, these densities are interrelated by the expressions

$$\tau(\mathbf{r}) = \xi(\mathbf{r}) - \frac{1}{4} \frac{\hbar^2}{2m} \nabla^2 \rho(\mathbf{r}), \quad \tau_1(\mathbf{r}) = \xi(\mathbf{r}) + \frac{1}{4} \frac{\hbar^2}{2m} \nabla^2 \rho(\mathbf{r}). \quad (5)$$

We now separate all densities into a smooth and an oscillating part:

$$\rho(\mathbf{r}) = \tilde{\rho}(\mathbf{r}) + \delta\rho(\mathbf{r}), \quad (6)$$

$$\tau(\mathbf{r}) = \tilde{\tau}(\mathbf{r}) + \delta\tau(\mathbf{r}), \quad (7)$$

$$\tau_1(\mathbf{r}) = \tilde{\tau}_1(\mathbf{r}) + \delta\tau_1(\mathbf{r}), \quad (8)$$

$$\xi(\mathbf{r}) = \tilde{\xi}(\mathbf{r}) + \delta\xi(\mathbf{r}). \quad (9)$$

The smooth parts are for differentiable potentials $V(\mathbf{r})$ given by the extended Thomas-Fermi (ETF model) in terms of gradients of $V(\mathbf{r})$. For billiard systems, where no gradient expansion of the potential exists, they are just given by their constant TF values. For the oscillating parts we have derived [1] a semiclassical expansion in terms of classical orbits which shall be examined analytically here for the circular billiard with radius R .

The potential of the circular billiard is defined by

$$V = 0 \quad \text{for} \quad 0 \leq r \leq R, \quad V = \infty \quad \text{for} \quad r > R, \quad (10)$$

where (r, ϕ) are polar coordinates. We solve the Schrödinger equation for this potential with the Dirichlet boundary condition $\psi_j(r = R, \phi) = 0$. $\{j\}$ are given by the set of the radial quantum numbers $n = 0, 1, 2, \dots$ and the angular-momentum quantum numbers $l = 0, \pm 1, \pm 2, \dots$. The eigenenergies and normalized wave functions are given [6] by

$$\begin{aligned} E_{nl} &= z_{nl}^2 E_0, & E_0 &= \hbar^2 / (2mR^2), \\ \psi_{nl}(r, \phi) &= c_{nl} J_l(z_{nl} r/R) e^{il\phi}. \end{aligned} \quad (11)$$

The normalization constants are $c_{nl} = [\sqrt{\pi} R J_{l+1}(z_{nl})]^{-1}$, where z_{nl} is the n -th zero of the cylindrical Bessel function $J_l(z)$. ψ_{nl} can be summed to yield the exact quantum-mechanical densities (1) – (3).

The smooth parts of the densities, which in billiard systems are independent of r , are given by their TF values \ddagger in terms of a smooth Fermi energy $\tilde{\lambda}$:

$$\tilde{\rho} = \rho_{\text{TF}} = \frac{m\tilde{\lambda}}{\pi\hbar^2} = \frac{1}{2\pi R^2} \left(\frac{\tilde{\lambda}}{E_0} \right), \quad \tilde{\tau} = \tau_{\text{TF}} = \frac{m\tilde{\lambda}^2}{2\pi\hbar^2} = \frac{1}{4\pi R^2} \left(\frac{\tilde{\lambda}^2}{E_0} \right). \quad (12)$$

Note that $\tilde{\tau}$ is the common smooth part of all three kinetic energy densities (2) – (4). From the Weyl expansion [7, 8] of the integrated level density given in (86), we can find the asymptotic expansion of the Fermi energy $\tilde{\lambda}(N)$ in powers of $N^{-1/2}$:

$$\tilde{\lambda}(N) = E_0 \left[2N + 2(2N)^{1/2} + \frac{4}{3} + \mathcal{O}(N^{-1/2}) \right]. \quad (13)$$

For the oscillating parts of the densities, we now reproduce the main formulae from [1] for the special case of $D = 2$ space dimensions and spherical symmetry when all densities only depend on the radial variable $r = |\mathbf{r}|$. To leading order in \hbar , the semiclassical expressions for the oscillating parts of the densities are given by

$$\delta\rho(r) \simeq \sum_{\gamma} \mathcal{A}_{\gamma}(\tilde{\lambda}, r) \cos \left[\frac{1}{\hbar} S_{\gamma}(\tilde{\lambda}, r) - \mu_{\gamma} \frac{\pi}{2} - \frac{3\pi}{4} \right], \quad (14)$$

$$\delta\tau(r) \simeq \frac{p_{\tilde{\lambda}}^2}{2m} \sum_{\gamma} \mathcal{A}_{\gamma}(\tilde{\lambda}, r) \cos \left[\frac{1}{\hbar} S_{\gamma}(\tilde{\lambda}, r) - \mu_{\gamma} \frac{\pi}{2} - \frac{3\pi}{4} \right], \quad (15)$$

$$\delta\tau_1(r) \simeq \frac{p_{\tilde{\lambda}}^2}{2m} \sum_{\gamma} \mathcal{A}_{\gamma}(\tilde{\lambda}, r) Q_{\gamma}(\tilde{\lambda}, r) \cos \left[\frac{1}{\hbar} S_{\gamma}(\tilde{\lambda}, r) - \mu_{\gamma} \frac{\pi}{2} - \frac{3\pi}{4} \right]. \quad (16)$$

The sum is over all closed orbits γ starting and ending in the point r . In principle, only *non-periodic* orbits (NPOs) contribute to the oscillating parts, but in connection with symmetry breaking at $r = 0$ and bifurcations at finite distances, also the contributions of periodic orbits (POs) must be included as discussed in section 4. The action function

\ddagger We note that the density ρ_{TF} in (12) cannot be normalized to the correct particle number N . The reason is that the constant TF density is not able to reproduce the sharp decrease of the quantum-mechanical density $\rho(r)$ near the boundary $r = R$, where it is forced to become zero.

$S_\gamma(\tilde{\lambda}, r) = S_\gamma(\tilde{\lambda}, r, r' = r)$ is gained from the general open action integral for an orbit starting at \mathbf{r} and ending at \mathbf{r}' at fixed energy $E = \tilde{\lambda}$

$$S_\gamma(\tilde{\lambda}, \mathbf{r}, \mathbf{r}') = \int_{\mathbf{r}}^{\mathbf{r}'} \mathbf{p}(\tilde{\lambda}, \mathbf{q}) \cdot d\mathbf{q}, \quad (17)$$

where $\mathbf{p}(\tilde{\lambda}, \mathbf{r})$ is the classical momentum in the point \mathbf{r} , for $V(\mathbf{r}) = 0$ given by

$$\mathbf{p}(\tilde{\lambda}, \mathbf{r}) = \frac{\dot{\mathbf{r}}}{|\dot{\mathbf{r}}|} \sqrt{2m\tilde{\lambda}}, \quad (18)$$

whose modulus is a constant of motion and denoted here by $p_\lambda = |\mathbf{p}(\tilde{\lambda}, \mathbf{r})|$. μ_γ is the Morse index that counts the number of conjugate points along the orbit [3] and will be discussed in section 3.7. The quantity $Q_\gamma(\tilde{\lambda}, r)$ appearing in (16) for $\delta\tau_1(r)$ is defined as

$$Q_\gamma(\tilde{\lambda}, r) = \frac{[\mathbf{p}(\tilde{\lambda}, \mathbf{r}) \cdot \mathbf{p}(\tilde{\lambda}, \mathbf{r}')]_{\gamma, \mathbf{r}'=\mathbf{r}}}{p_\lambda^2} = \cos[\theta(\mathbf{p}, \mathbf{p}')]_\gamma, \quad (19)$$

where \mathbf{p} and \mathbf{p}' are the short notations for the initial and final momentum, respectively, of the orbit γ at the point \mathbf{r} . These are obtained also from the action integral (17) by

$$\nabla_{\mathbf{r}} S_\gamma(\tilde{\lambda}, \mathbf{r}, \mathbf{r}') \Big|_{\mathbf{r}=\mathbf{r}'} = -\mathbf{p}, \quad \nabla_{\mathbf{r}'} S_\gamma(\tilde{\lambda}, \mathbf{r}, \mathbf{r}') \Big|_{\mathbf{r}=\mathbf{r}'} = \mathbf{p}'. \quad (20)$$

Since $Q_\gamma(\tilde{\lambda}, r)$ in (19) depends on the angle θ between \mathbf{p} and \mathbf{p}' , it may be called the ‘‘momentum mismatch function’’, being $Q_\gamma = +1$ for POs with $\mathbf{p} = \mathbf{p}'$ and $Q_\gamma = -1$ for self-retracing NPOs with $\mathbf{p} = -\mathbf{p}'$.

The common semiclassical amplitude $\mathcal{A}_\gamma(\tilde{\lambda}, r)$ in all densities is given by

$$\mathcal{A}_\gamma(\tilde{\lambda}, r) = \frac{2m}{\pi p_\lambda} \frac{\sqrt{|\mathcal{D}_{\perp\gamma}(\tilde{\lambda}, r)|}}{\sqrt{2\pi\hbar} T_\gamma(\tilde{\lambda}, r)}, \quad \mathcal{D}_{\perp\gamma}(\tilde{\lambda}, r) = \left(\frac{\partial p_\perp}{\partial r'_\perp} \right) \Big|_{\mathbf{r}'=\mathbf{r}}. \quad (21)$$

Here $T_\gamma(\tilde{\lambda}, r) = dS_\gamma(E, r)/dE|_{E=\tilde{\lambda}}$ is the running time of the orbit, and $\mathcal{D}_{\perp\gamma}$ its stability determinant calculated from the components p_\perp and r'_\perp *transverse* to the orbit γ of the initial momentum and final coordinate, respectively. We shall in the following express the amplitudes defined in (21) through the Jacobians \mathcal{J}_γ , which are defined as the inverse stability determinants, and omit the Fermi energy $\tilde{\lambda}$ from all arguments:

$$\mathcal{A}_\gamma(r) = \frac{2m}{p_\lambda \pi \sqrt{2\pi\hbar} T_\gamma(r)} \frac{1}{\sqrt{|\mathcal{J}_\gamma(r)|}}, \quad \mathcal{J}_\gamma(r) = \left(\frac{\delta r'_\perp}{\delta p_\perp} \right) \Big|_{\mathbf{r}'=\mathbf{r}}. \quad (22)$$

From (14) and (15) using $p_\lambda^2/2m = \tilde{\lambda}$, we find immediately the semiclassical relation

$$\delta\tau(r) \simeq \tilde{\lambda} \delta\rho(r), \quad (23)$$

which is the *local virial theorem* discussed extensively in [2] (valid here for $V(\mathbf{r}) = 0$). Note, however, that this theorem fails at the boundary $r = R$ (cf. section 4.3).

It has been observed in [2] (see also figures 12 and 13) that for systems with spherical symmetry for $D > 1$ (except harmonic oscillators), there exist two types of oscillations: (i) regular, short-ranged oscillations due to the linear orbits in the radial direction, and (ii) irregular, long-ranged oscillations due to the non-linear orbits (which do not exist

in harmonic oscillators). Like in [2], we therefore decompose the oscillating parts of the densities (14) – (16) in the following way (in obvious notation)

$$\begin{aligned}\delta\rho(r) &= \delta_r\rho(r) + \delta_{\text{irr}}\rho(r), \\ \delta\tau(r) &= \delta_r\tau(r) + \delta_{\text{irr}}\tau(r), \\ \delta\tau_1(r) &= \delta_r\tau_1(r) + \delta_{\text{irr}}\tau_1(r).\end{aligned}\tag{24}$$

The contribution of the linear NPOs to the particle density (14) near $r = 0$ can be summed over all repetitions k and has already been given in [1, 2]. For the present system it becomes:

$$\delta_r\rho(r) = (-1)^{M-1} \frac{m}{\hbar T_{r1}(\tilde{\lambda})} J_0(2rp_\lambda/\hbar). \quad (r \ll R)\tag{25}$$

Here $J_0(z)$ is the cylindrical Bessel function of order zero, M is the number of filled “main shells” to be discussed in section 5, and $T_{r1} = 4mR/p_\lambda$ is the period of the diametrical PO. This result will be generalized to larger radii in section 4.1.

The contribution of the linear NPOs to the kinetic energy densities are now easily obtained from the general equations (14) – (16). For $\delta_r\tau(r)$ we may just use the local virial theorem (23) to get an expression valid for small r . Since $Q_\gamma(r) = -1$ for all linear NPOs, we get the relation [1]

$$\delta_r\tau_1(r) = -\delta_r\tau(r), \quad (r \ll R)\tag{26}$$

again valid for small r .

In the following section, we shall classify all closed orbits in the circular billiard and derive their analytical properties introduced above.

3. Closed orbits in the circular billiard

3.1. Classification and symmetries of orbits

We may classify the NPOs in the circular billiard in the same way as it has been done for the POs by Balian and Bloch [9]. They specified them by pairs of integers (v, w) , where v is the number of reflections at the boundary and w is the winding number around the center ($r = 0$). If v and w have a common divisor $k > 1$, the number k is the number of repetitions of the primitive orbit (which by definition has $k = 1$). The librating diametrical POs have by definition the winding number $v = w$. For the non-linear NPOs, there generally exist no repetitions (i.e., $k = 1$), except at the points $r = 0$ and $r = R$ where they become periodic. Repetitions of non-linear NPOs do occur at specific isolated points $0 < r < R$ at which they become identical with POs or fractions thereof. In the calculation of the semiclassical densities we found, however, that these repetitions are practically negligible because they lead to rather long orbits. For the linear radial NPOs, a generalized repetition number $k \geq 0$ will be defined in section 3.6.

All orbits starting and ending in a fixed point $r > 0$ are isolated and occur in discrete degenerate pairs corresponding to the time-reversal symmetry. This holds also for the

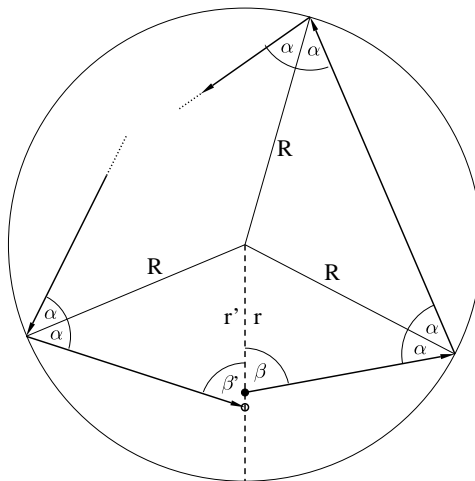


Figure 1. Geometry of an arbitrary orbit in the circular billiard with radius R , starting at distance r (dot) and ending at distance r' (circle) from the center along the same radius vector (shown by the vertical dashed line).

librating (i.e., radial) POs. § All orbits starting and ending at the origin $r = 0$ form families of continuously degenerate orbits, since they can be rotated about arbitrary finite angles around the origin due to the $U(1)$ symmetry of the system. This has consequences for their semiclassical amplitudes, as discussed in section 4.1.

3.2. Geometry of an arbitrary orbit with v reflections and winding number w

We now study the geometry of an arbitrary orbit, as illustrated in figure 1. Let the particle start from a point r (black dot) on a radius vector $0 < r < R$ (vertical dashed line). Let β be the starting angle with respect to that radius vector. Let β' be the final angle at which the particle returns to the point r' (circle) on the same radius vector after v reflections at the boundary and winding w times around the origin. Both β and β' are chosen to lie *inside* the polygon formed by the orbit. The relation between β , β' and the reflection angle α at the boundary then is

$$\beta' = (1 - w) 2\pi + (v - 1) \pi - 2v\alpha - \beta. \quad (27)$$

Note that according to our definition, all angles α , β and β' are non-negative. Moreover, they are restricted in all cases by $0 \leq \alpha < \pi/2$ and $0 \leq \beta, \beta' \leq \pi$. The lengths r and r' can be expressed in terms of these angles and R by

$$r = R \frac{\sin \alpha}{\sin \beta}, \quad (28)$$

$$r' = R \frac{\sin \alpha}{\sin \beta'}. \quad (29)$$

§ This is different in the trace formula for the level density: there one integrates over all r and thereby includes automatically all pairs of librations starting in opposite directions, so that librations must only be counted once

The condition for an orbit to be closed, $r = r'$, leads to $\sin \beta = \sin \beta'$ which has only two solutions in the physically interesting domain $\beta, \beta' \in [0, \pi]$, namely:

- a) $\beta' = \beta$, giving in general a NPO (which, however, can become periodic in an isolated point where $\beta' = \beta = \pi/2$), and
- b) $\beta' = \pi - \beta$, always giving a PO.

From (28) we can express β implicitly in terms of r and α by the following relations

$$\cos \beta = \pm \frac{R}{r} \sqrt{\frac{r^2}{R^2} - \sin^2 \alpha}, \quad \cot \beta = \pm \frac{1}{\sin \alpha} \sqrt{\frac{r^2}{R^2} - \sin^2 \alpha}. \quad (30)$$

The signs above must be taken to be positive if $\beta \leq \pi/2$ and negative if $\beta \geq \pi/2$.

3.3. Non-periodic orbits

Inserting $\beta' = \beta$ into (27), the relation between β and α becomes

$$\beta = (1 - w)\pi + (v - 1)\pi/2 - v\alpha. \quad (31)$$

Inserting (31) into (28) yields r as a function of α :

$$r(\alpha) = (-1)^w R \frac{\sin \alpha}{\cos(v\pi/2 - v\alpha)}, \quad (32)$$

which in general cannot be inverted explicitly. In order to find all NPOs in the circular billiard, it is sufficient to look for all real solutions $\alpha(r)$ of the inverse of equation (32) in the physical range $0 \leq \alpha \leq \pi/2$. Upon variation of $r \in [0, R]$ for a fixed pair (v, w) , U(1) symmetry breaking at $r = 0$ creates non-linear NPOs, while bifurcations of some NPOs occur at specific points $r_b > 0$, whereby new NPOs or POs are created. It turns out that the linear radial NPOs and the diametric PO are the prime generators of many other closed orbits in the circular billiard. The remaining NPOs are created in tangent bifurcations. The bifurcation scenarios are discussed in detail in section 3.6.

The NPOs are symmetric about the radius vector containing the point r . They are doubly degenerate due to the time reversal symmetry, which here is identical to the reflection symmetry, except for $v = 2, w = 1$ in the limiting case $r = 0$ ($\alpha = 0, \beta = \pi/2$), in which case the orbit becomes linear and is mapped onto itself by time reversal.

The length of the orbit (v, w) becomes

$$L_{v,w}(r) = 2(vR \cos \alpha + r \cos \beta). \quad (33)$$

The explicit dependence of (33) on v and w is obtained when inserting (31) for β . Note that, because of the implicit r dependence of α and β , the formula (33) does not reveal the full (non-linear) dependence on the radius r .

At $r = R$, the NPOs become periodic with $v + 1$ or $v - 1$ reflections (see the systematics in section 3.6). In this case we have $\beta = \alpha$ or $\beta = \pi - \alpha$, and $L_{v,w}(r = R) = 2R(v \pm 1) \cos \alpha$. In the notation of Balian and Bloch [9], the half polar angle covered between two successive reflections of an orbit with v reflections is $\phi_{v,w} = w\pi/v$. The lengths then become $L_{v,w}(r = R) = 2R(v \pm 1) \sin \phi_{v \pm 1, w}$.

It is important to realize that the function $L_{v,w}(\alpha)$ given in (33) is *stationary with respect to α* , at a fixed value of r , *precisely for the NPOs obeying the relation (28)*.

Indeed, with the extra condition (31) which implies $\partial\beta/\partial\alpha = -v$, we find the stationary condition to lead to

$$\left. \frac{dL_{v,w}(\alpha)}{d\alpha} \right|_r = 2v(r \sin \beta - R \sin \alpha) = 0, \quad (34)$$

which is identical with (28). For later reference, we give here also the second derivative:

$$\left. \frac{d^2 L_{v,w}(\alpha)}{d\alpha^2} \right|_r = -2vR \cos \alpha \left(1 + v \frac{r \cos \beta}{R \cos \alpha} \right). \quad (35)$$

For the calculation of the Jacobian $\mathcal{J}_\gamma = \mathcal{J}_{v,w}$ defined in (22), we make a small variation of the initial momentum by a small variation $\delta\beta$ of the starting angle. The reflection angle then will be $\alpha' = \alpha + \delta\alpha$. From (28) with fixed r , we obtain

$$\delta\alpha = \frac{r \cos \beta}{R \cos \alpha} \delta\beta. \quad (36)$$

The particle will then return to the point $r + \delta r'$ with the angle $\beta' + \delta\beta'$, where

$$\delta\beta' = -\delta\beta - 2v\delta\alpha. \quad (37)$$

From (29) we obtain the increment $\delta r'$ as

$$\delta r' = \frac{R}{\sin \beta} (\cos \alpha \delta\alpha - \sin \alpha \cot \beta \delta\beta'). \quad (38)$$

Noting that the change of the starting transverse momentum is $\delta p_\perp = p_\lambda \delta\beta$ and the change of the final transverse distance is $\delta r'_\perp = \delta r' \sin \beta$, we obtain the Jacobian $\mathcal{J}_{v,w}$ as

$$\mathcal{J}_{v,w}(r) = \frac{R}{p_\lambda} \left[\sin \alpha \cot \beta + \frac{r}{R} \cos \beta (1 + 2v \tan \alpha \cot \beta) \right]. \quad (39)$$

Using (28) we can rewrite it in the form

$$\mathcal{J}_{v,w}(r) = \frac{2r}{p_\lambda} \cos \beta \left[1 + v \frac{r \cos \beta}{R \cos \alpha} \right]. \quad (40)$$

Like for the lengths (33), the explicit dependence of (39) and (40) on v and w comes through (31), and their full r dependence is not revealed. At $r = R$ we obtain the values

$$\mathcal{J}_{v,w}(r = R) = \frac{2R}{p_\lambda} (v \pm 1) \sin \phi_{v\pm 1,w}. \quad (41)$$

The Jacobian $\mathcal{J}_{v,w}(r)$ becomes zero, and therefore the amplitude $\mathcal{A}_{v,w}$ defined by (22) diverges, at three types of critical points:

- 1) $r = 0$: this corresponds to the caustic point of the families of degenerate orbits. Making $r > 0$ leads to U(1) *symmetry breaking*.
- 2a) $\cos \beta = 0$: this corresponds to a point for which the starting and ending angle is $\beta = \pi/2$; the orbit then becomes periodic with v reflections. This point is the caustic point $r_{v,w}^{\text{PO}} = R \cos \phi_{v,w}$ of the PO family $(v, w, 1)$, an isolated member of which is created there in a *pitchfork bifurcation* (see section 3.6).

2b) The term in square brackets is zero, implying

$$v r \cos \beta = -R \cos \alpha. \quad (42)$$

This is fulfilled in the following cases (cf. section 3.6):

a) for the radial type “+” orbits ($\beta = \pi$, $\alpha = 0$) with $(v, w) = (2k + 1, k)$, $k > 0$, which we call $L_+^{(k)}$ (cf. section 3.5) in the points $r_k = R/v = R/(2k + 1)$ at which non-linear NPOs $(2k + 1, k)$ are created in a *pitchfork bifurcation*, or

b) for non-linear orbits which are born in pairs (v, w) , $(v, w)'$ in a *tangent bifurcation* at a critical point $r_{v,w}$ which corresponds to a minimum of the function $r(\alpha)$ in (28).

This is found from the slope function

$$r'(\alpha) = \frac{dr(\alpha)}{d\alpha} = \frac{R}{\sin^2 \beta} [\cos \alpha \sin \beta + v \sin \alpha \cos \beta]. \quad (43)$$

The condition $r'(\alpha = 0)$ leads, indeed, to (42).

3) $r_0 = R$: this happens exclusively for the primitive “+” orbit (1,0) which is responsible for the Friedel oscillations near the surface [2].

The regularizations of the diverging amplitudes, using standard uniform approximations for symmetry breaking and bifurcations, will be discussed in section 4.2.

The momentum mismatch needed to obtain the density $\delta\tau_1(r)$ in (16) becomes

$$Q_{v,w}(r) = \mathbf{p} \cdot \mathbf{p}'/p^2 = -\cos(2\beta). \quad (44)$$

We stress that the results (33), (40) and (44) also hold for the radial orbits with $\alpha = 0$ and $\beta = 0$ or π , which are discussed specifically in section 3.5, and for which we have the relation $v = 2k + 1$.

3.4. Periodic orbits

For $\beta' = \pi - \beta$, we obtain POs. At any point $r > 0$, they are isolated. If $\beta' = \beta = \pi/2$, they are symmetric about the radius vector; if $\beta \neq \pi/2$, they exist in two degenerate versions related to each other by reflection at the radius vector. Each of them is doubly degenerate due to time reversal symmetry, except for the diameter orbit $v = 2$.

Inserting $\beta' = \pi - \beta$ into (27), the angle β falls out and we obtain the reflection angle $\alpha_{v,w}$ of the POs:

$$\alpha = \alpha_{v,w} = \left(\frac{v - 2w}{2v} \right) \pi = \frac{\pi}{2} - \frac{w\pi}{v}, \quad (45)$$

and hence

$$\phi_{v,w} = \frac{\pi}{2} - \alpha_{v,w} = \frac{w\pi}{v}, \quad (46)$$

as given by Balian and Bloch [9]. The lengths of the orbits which are, of course, independent of the starting point r , become

$$L_{v,w}^{\text{PO}} = 2vR \sin \phi_{v,w}. \quad (47)$$

Note that this formula follows from (33) with (46) and $\cos \beta = 0$.

For the calculation of the Jacobians, we again use equation (36), but the equation (38) becomes for POs, with $\sin \beta' = \sin \beta$ and $\cos \beta' = -\cos \beta$,

$$\delta r' = \frac{R}{\sin \beta} (\cos \alpha \delta \alpha + \sin \alpha \cot \beta \delta \beta'), \quad (48)$$

where $\delta \beta'$ is given in (37). With this, we obtain the Jacobians

$$\mathcal{J}_{v,w}(r)^{\text{PO}} = -\frac{2v}{Rp_\lambda} \frac{1}{\cos \alpha} (r^2 - R^2 \sin^2 \alpha) = -\frac{2v}{Rp_\lambda} \frac{(r^2 - R^2 \cos^2 \phi_{v,w})}{\sin \phi_{v,w}}. \quad (49)$$

The negative sign in front of the last expression above is opposite to that given in [10], where a trace formula for the level density of the circular billiard has been derived. It was, however, compensated in [10] by a different book-keeping of the phases in the computation of the Maslov index [see our remark after equation (57) below in section 3.7.] Comparing (41) and (49), we note that $\mathcal{J}_{v,w}^{\text{NPO}}(r = R) = -\mathcal{J}_{v+1,w}^{\text{PO}}(r = R)$. At the caustic points $r_{v,w}^{\text{PO}}$ given by

$$r_{v,w}^{\text{PO}} = R \cos \phi_{v,w}, \quad (50)$$

the Jacobian becomes zero. These are, in fact, the critical points at which all non-linear POs (v, w) are created from NPOs (v, w) by a pitchfork bifurcation (see section 3.6).

Trivially, the momentum mismatch is $Q_{v,w}(r) = 1$ for all POs at all points except the reflections points on the boundary. At these, $Q_{v,w}(R)$ can be evaluated as the limit $r \rightarrow R$ of the expression (44) for the (suitably chosen) NPOs.

3.5. Linear radial orbits and bifurcations of POs

There are only two kinds of linear NPOs starting at any point $0 < r < R$ in the radial direction. They correspond to the only NPOs that exist in one-dimensional systems. Like in [1], we call the “+” orbits those which start in the outwards direction and are reflected at the nearest turning point, and the “−” orbits those which start in the inwards direction and are reflected at the opposite turning point. The primitive “+” and “−” orbits have only $v = 1$ reflection at the boundary; by definition their repetition number is $k = 0$. Using the geometry of section 3.3, we have $\alpha = 0$ and $\beta = \pi$ or $\beta = 0$ for the “+” or “−” orbit, respectively. To both orbits, one may add $k > 0$ full librations between the two opposite turning points; we call k their “repetition number”. Their reflection number then is $v = 2k + 1$. In order to be consistent with (31), we define their winding numbers to be $w = k$ for the “+” and $w = k + 1$ for “−” orbits. Because both v and w are determined by k , the repetition number k is sufficient to characterize the linear NPOs uniquely. We shall denote them here by the symbol $L_{\pm}^{(k)}$. At $r = R$, the orbits $L_{+}^{(k)}$ with $k > 0$ become identical with the k -th repetitions of the primitive PO (2,1), while the orbits $L_{-}^{(k)}$ for all k become its $(k + 1)$ -th repetitions ($2k + 2, k + 1$).

The formulae (33), (40) and (44) can be used with $\cos \beta = \mp 1$ for the $L_{\pm}^{(k)}$ orbits. One of their characteristic features is that they have opposite initial and final momenta, $\mathbf{p}' = -\mathbf{p}$, so that $Q_{\pm}^{(k)}(r) = -1$ at all points. Their lengths become

$$L_{\pm}^{(k)}(r) = 2[(2k + 1)R \mp r]. \quad (51)$$

For the Jacobians we obtain

$$\mathcal{J}_{\pm}^{(k)}(r) = \frac{2}{Rp_{\lambda}} r[(2k+1)r \mp R]. \quad (52)$$

Both Jacobians are zero at $r = 0$ where the “+” and “−” orbits become identical and form a rotationally degenerate family, as discussed in more detail in section 4.1. Furthermore, the $L_{+}^{(k)}$ orbits have zero Jacobians at $r_k = R/(2k+1)$. For the primitive “+” orbit, this gives the turning point $r_0 = R$ at the boundary, where the divergence of the semiclassical amplitude is removed by the uniform approximation discussed in section 4.3. At the points $r_k = R/(2k+1)$ with $k > 0$, *non-linear* NPOs with $2k+1$ reflections at the boundary are born from the $L_{+}^{(k)}$ orbits in pitchfork bifurcations. The example of $k = 1$, where the new NPO here is called the Λ orbit (see also figure 2), will be discussed explicitly in section 4.2 along with the corresponding uniform approximation for its semiclassical amplitude.

3.6. Creation and systematics of non-linear orbits

The properties of all closed orbits in the circular disk are obtained by systematically inverting (32) for all (v, w) and inserting the resulting angles $\alpha(r)$, $\beta(r)$ at each point r into the equations (33), (40) and (44). As already mentioned, bifurcations of the orbits occur under variation of r , at which new orbits are created. Furthermore, the $U(1)$ symmetry of the continuously degenerate orbit families existing at $r = 0$ is broken when r becomes > 0 , whereby non-linear NPOs are created. In fact, we find that all non-linear NPOs are created either (i) by the k -th repetition of the diametrical PO $(v, w) = (2k, k)$ (with $k = 1, 2, \dots$) by $U(1)$ *symmetry breaking*, or (ii) by the orbits $L_{+}^{(k)}$ by *pitchfork bifurcations*, or (iii) pairwise by *tangent bifurcations*. All non-linear POs are created by pitchfork bifurcations from non-linear NPOs.

The detailed systematics are as follows. (We include here also the Morse indices whose determination is discussed in section 3.7.)

- Non-linear orbits have $v \geq 2$ and $1 \leq w \leq \lfloor \frac{v}{2} \rfloor$, where $\lfloor x \rfloor$ is the integer part of x .
- NPOs with *even* v and *maximum* w , i.e. $(v, w) = (2k, k)$, are created from the family of POs $(2k, k)$ (i.e., the k -th repetitions of the diameter orbit) by $U(1)$ *symmetry breaking* at $r = 0$ which is the caustic point of the family. These new NPOs exist at all distances $0 \leq r \leq R$. Their Morse index is $\mu = 3v$. At $r = R$ they become equal to the POs $(2k+1, k)$.
- NPOs with *odd* v and *maximum* w , i.e. $(v, w) = (2k+1, k)$, are created from the radial $L_{+}^{(k)}$ orbits by a *pitchfork bifurcation* at $r_k = R/(2k+1)$ which are critical points of $\mathcal{J}_{+}^{(k)}(r)$. They exist at all distances $r_k \leq r \leq R$; at $r = R$ they become equal to the POs $(2k+2, k)$. At $r = r_{v,w}^{\text{PO}}$ they create the PO $(2k+1, k)$ in a further *pitchfork bifurcation*, whereby $r_{v,w}^{\text{PO}}$ is the caustic radius (50) of that PO family. The Morse index is $\mu = 6k+2$ for $r_k < r < r_{v,w}^{\text{PO}}$ and $\mu = 6n+3$ for $r_{v,w}^{\text{PO}} < r < R$.
- All remaining NPOs are created in pairs (v, w) , $(v, w)'$ (with identical values of v and w) by *tangent bifurcations* at critical points $r_{v,w}$ (with $0 < r_{v,w} < R$) where the

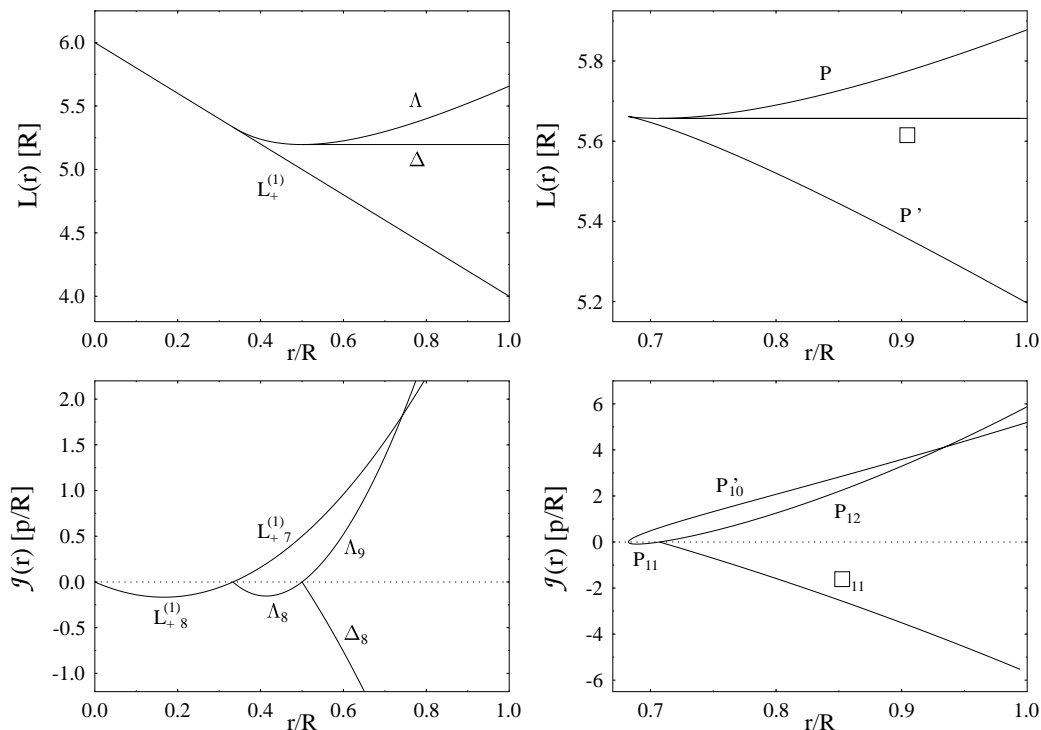


Figure 2. Bifurcations of the NPOs $(v, w) = (3, 1)$ ($L_+^{(1)}$ and Λ) and the triangular PO $(3, 1)$ (Δ) (left panels), and of the NPOs $(v, w) = (4, 1)$ (P), $(4, 1)'$ (P') and the square PO $(4, 1)$ (\square) (right panels). *Top:* lengths $L_{v,w}(r)$, *bottom:* Jacobians $\mathcal{J}_{v,w}(r)$. In the lower panels, the subscripts of the orbit symbols indicate their Morse indices.

Jacobian $\mathcal{J}_{v,w}$ becomes zero [cf. equations (43), (42) and (40)]. They exist only for $r_{v,w} \leq r \leq R$. The points $r_{v,w}$ occur as minima of the function $r(\alpha)$ in (32). The two orbits correspond to the two branches of the inverse function $\alpha(r)$, whereby the orbit (v, w) has the slope $r'(\alpha) > 0$ and the orbit $(v, w)'$ has the slope $r'(\alpha) < 0$. They have the following properties and behaviors:

- The orbit (v, w) creates the PO (v, w) by *pitchfork bifurcation* at the caustic radius $r_{v,w}^{\text{PO}} > r_{v,w}$. Its Morse index is $\mu = 3v - 1$ for $r_{v,w} < r < r_{v,w}^{\text{PO}}$ and $\mu = 3v$ for $r_{v,w}^{\text{PO}} < r < R$. At $r = R$, the NPO (v, w) becomes equal to the PO $(v + 1, w)$.
- The orbit $(v, w)'$ undergoes no further bifurcation. Its Morse index is $\mu = 3v - 2$ at all radii $r_{v,w} < r < R$. At $r = R$, the NPO $(v, w)'$ becomes equal to the PO $(v - 1, w)$.

In figure 2 we illustrate some of the bifurcation scenarios. In the upper panels we show the lengths $L_{v,w}(r)$ and in the lower panels the Jacobians $\mathcal{J}_{v,w}(r)$ of some orbits as functions of the starting point r . In the left panels, the linear orbit $L_+^{(1)}$ is seen to undergo a pitchfork bifurcation at $r = R/3$, at which the non-linear orbit $\Lambda(v, w) = (3, 1)$ is created. At $r = R/2$, the orbit Λ undergoes a pitchfork bifurcation at which the triangular PO $(3, 1)$ (noted as Δ) is born. In the right panels, we see the creation of a pair of orbits $P(4, 1)$ and $P'(4, 1)'$ by a tangent bifurcation at $r_{4,1} = 0.682489R$, to

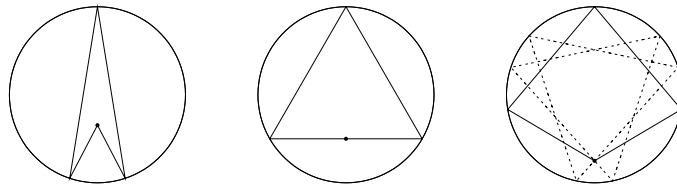


Figure 3. Shapes of the NPO Λ (3,1), shown by the solid lines, at the starting points $r = 0.345R$, $r = R/3$ and $r = 0.75R$ (from left to right). In the right panel, the dashed lines show the shape of the triangle PO Δ , which exists in two versions lying symmetric to the diameter that contains the starting point r (black dot).

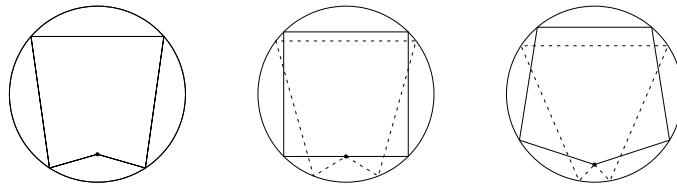


Figure 4. Shapes of NPOs P (4,1) (solid lines) and P' (4,1)' (dashed lines) with starting points $r = r_{4,1}$, $r = R/\sqrt{2}$ and $r = 0.8R$ (from left to right).

the left of which they do not exist. The orbit P undergoes a pitchfork bifurcation at $r_{4,1}^{\text{PO}} = R/\sqrt{2}$, at which the squared PO (4,1) (noted as \square) is born. In the lower panels, the subscripts of the orbit symbols indicate their Morse indices μ .

In figure 3 we show the shape of the Λ orbit at three starting points (from left to right): at $r = 0.345R$ shortly after its bifurcation from the $L_+^{(1)}$ orbit, at $r = R/3$ (i.e. at the pitchfork bifurcation where it is identical with the PO Δ), and at $r = 0.75R$ together with the two POs Δ passing through the same point. Three shapes of the orbits P and P' are shown in figure 4, chosen (from left to right) at the starting point $r = r_{4,1}$ (tangent bifurcation, where they are identical), at $r = R/\sqrt{2}$ (pitchfork bifurcation, where P is identical with \square), and at $r = 0.8R$. Analytical expressions for the lengths and Jacobians of the orbits Λ , P and P' are given in the appendix.

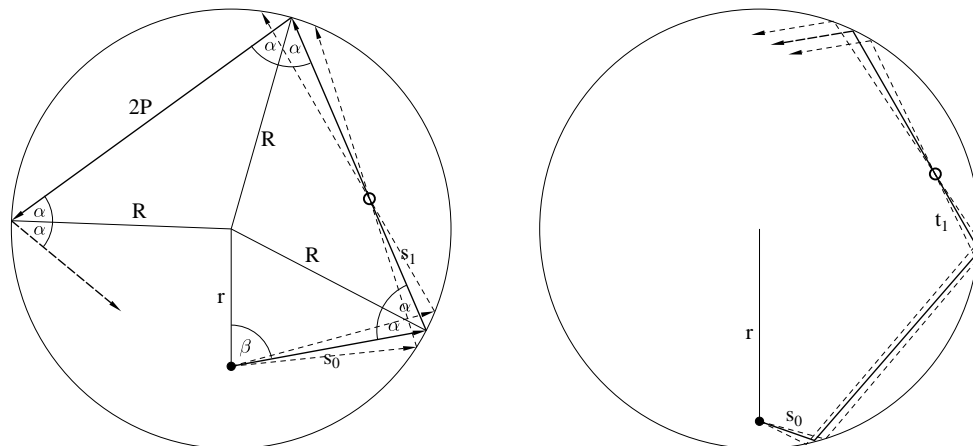


Figure 5. Small perturbations (thin dashed lines) of an orbit (thick solid line) starting at a point r (black dot) with distance s_0 to the first reflection point. The first conjugate point is shown by a circle. *Left:* $s_0 > 2P/3$; here the conjugate point occurs at distance s_1 from the first reflection point. *Right:* $s_0 < 2P/3$; here the conjugate point occurs only after the second reflection at distance t_1 from the second reflection point.

3.7. Calculation of Morse indices

Following Gutzwiller [3], we calculate the Morse index of a given orbit by counting the number of *conjugate points* along the orbit. These are by definition the points \mathbf{r}_c in which a fan of infinitesimally perturbed orbits, all starting at the same point \mathbf{r}_0 , intersects itself. To this number, one has to add twice the number of reflections at the boundary, since each hard-wall reflection yields a phase shift of π , while each conjugate point that does not lie on the boundary yields a semiclassical phase $\pi/2$ [3] (except for multiple conjugate points which can occur in the presence of higher continuous symmetries in $D > 2$; this does not happen in the present system).

We illustrate the procedure of determining the conjugate points in the circular billiard in figure 5 for an arbitrary non-linear orbit; the resulting formulae (55), (56) hold, however, also for the linear NPOs. Let the orbit start at a distance r from the center. Let the starting angle be β , as in figure 1, and denote the distance of the starting point to the first reflection point by s_0 . Let the distance of two successive reflections of the orbit be $2P$, so that we have

$$P = R \cos \alpha. \quad (53)$$

We now consider a fan of orbits, starting at the same point r , with infinitesimally perturbed angles $\beta' = \beta + \delta\beta$. These perturbed orbits will intersect in a conjugate point, shown in figure 5 by a circle. For $s_0 > 2P/3$, the first conjugate point is located on the next portion of the trajectory at a distance s_1 from the first reflection point, as shown in the left panel of figure 5. For $s_0 < 2P/3$, the first conjugate point does not lie on the next portion of the unperturbed trajectory, but on the subsequent one, i.e., between the second and third reflections, at a distance t_1 from the second reflection

point (see the right panel of figure 5).

The calculation of the distances s_1 and t_1 is elementary, using differential calculus and trigonometry. The perturbed reflection angle at the boundary is $\alpha' = \alpha + \delta\alpha$ with

$$\delta\alpha = \frac{r}{R} \frac{\cos\beta}{\cos\alpha} \delta\beta, \quad (54)$$

as follows from (28) and (31). For infinitesimal perturbations ($\delta\beta \rightarrow 0$), s_1 and t_1 must be independent of $\delta\beta$ due to the definition of a conjugate point. This leads, after some algebra using (53) and $r \cos\beta = s_0 - P$, to the following values which are consistent with the findings of [11]:

$$s_1 = P - \frac{P(s_0 - P)}{(2s_0 - P)} \quad \text{for} \quad s_0 \geq \frac{2}{3}P, \quad (55)$$

$$t_1 = P - \frac{P(P - s_0)}{(3P - 4s_0)} \quad \text{for} \quad s_0 \leq \frac{2}{3}P. \quad (56)$$

Special cases are the following: (i) $s_0 = 2P/3 \Rightarrow s_1 = 2P$ or $t_1 = 0$. (ii) $s_0 = 0 \Rightarrow t_1 = 2P/3$. (iii) $s_0 = 2P \Rightarrow s_1 = 2P/3$. (iv) $s_0 = P \Rightarrow s_1 = P$. In this last case, the starting point is a *caustic point* of a family of degenerate orbits due to the rotational U(1) symmetry. We note that these caustic points, common to families of rotationally degenerate (periodic or non-periodic) orbits, never coincide with conjugate points unless they are chosen as starting points (which, however, one should avoid as emphasized below).

The successive conjugate points s_n or t_n with $n = 2, 3, \dots$ along an orbit are then found iteratively by taking the previous conjugate points as new starting points, evaluating their distance s'_0 to the next reflection point, and using the relevant formula of (55), (56) with s_0 replaced by s'_0 .

As stated above, the total Morse index μ for a given orbit is obtained by adding to the number of conjugate points twice the number v of reflections at the boundary. We emphasize that for the resulting Morse index to be well defined, the starting point may *not* be any critical (caustic, conjugate or reflection) point (cf. section 4).

For the POs (v, w) , we find in this way that the number of conjugate points is always $v - 1$, i.e., one less than the number of reflections. Including the contributions from the reflections, their total Morse index therefore is given by

$$\mu_{v,w}^{\text{PO}} = 3v - 1. \quad (57)$$

This Morse index has been used implicitly in the derivation of the trace formula for the level density of the circular billiard in [10]. The calculation there was, however, done with a different book-keeping of the phases, absorbing the negative overall sign of $\mathcal{J}_{v,w}$ in our result (49) into the Maslov index given in [10].

For the linear NPOs $L_{\pm}^{(k)}$, we obtain the following Morse indices:

$$\begin{aligned} \mu_+^{(k)} &= 6k + 2 \quad \text{for} \quad r < r_k = R/(2k + 1), \\ \mu_+^{(k)} &= 6k + 1 \quad \text{for} \quad r > r_k = R/(2k + 1), \\ \mu_-^{(k)} &= 6k + 3. \end{aligned} \quad (58)$$

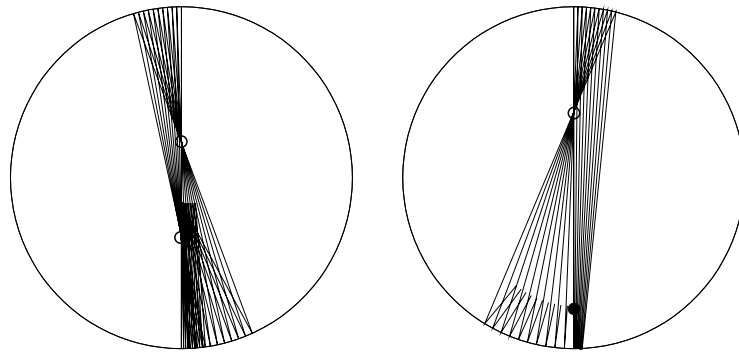


Figure 6. Orbit $L_+^{(1)}$ with starting point at $r = 0.15R$ (left) and $r = 0.75R$ (right). Fans of small perturbations with different starting angles exhibit the positions of the conjugate points. The total Morse indices become $\mu = 6 + 2 = 8$ (left, with two conjugate points) and $\mu = 6 + 1 = 7$ (right, with one conjugate point), in agreement with the general result (58).

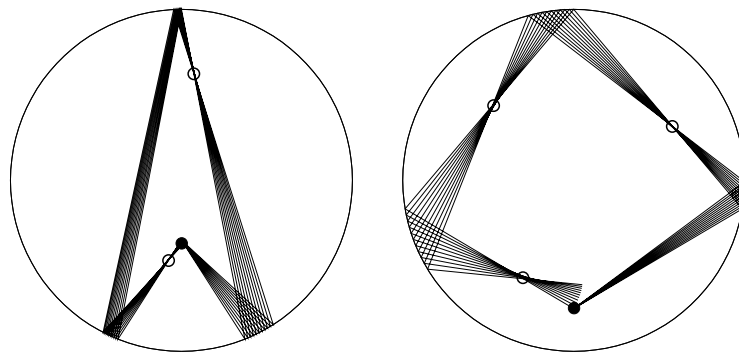


Figure 7. Same as figure 6 for the orbit Λ with starting point at $r = 0.35R$, giving $\mu = 6 + 2 = 8$ (left, with two conjugate points) and $r = 0.75R$ giving $\mu = 6 + 3 = 9$ (right, with three conjugate points).

For the non-linear NPOs, no single general formulae can be found. We have, however, given the Morse indices of the various types of NPOs in their systematics at the end of section 3.6.

The geometric construction of the conjugate points for the orbit $L_+^{(1)}$ is illustrated in figure 6, and for the orbit Λ , whose bifurcation is shown in figure 2 and further discussed in section 4.2, in figure 7.

4. Regularizations of semiclassical amplitudes

At the critical points of $\mathcal{J}_{v,w}(r)$ discussed in the previous section, the semiclassical amplitudes $\mathcal{A}_\gamma(\tilde{\lambda}, r)$ in the equations (14) – (16) for the spatial densities diverge. The reason for these divergences can be traced back to a break down of approximate stationary-phase integrations used in the derivation of Gutzwiller’s semiclassical Green function [3] that underlies also our semiclassical theory of spatial density oscillations [1]. In order to regularize the amplitudes, we resort to standard uniform approximations that have been developed for semiclassical trace formulae for the level density in terms of POs in connection with symmetry breaking [12, 13, 14, 15] and bifurcations [12, 14, 16, 17, 18].

For symmetry breaking, the uniform approximations in general depend not only on the particular symmetry that is broken, but also on the way in which a system is perturbed [15, 19]. For U(1) symmetry breaking, however, the uniform approximation developed in [13, 14] is universal and can be readily applied in section 4.1. For bifurcations, on the other hand, the uniform approximations do not depend on the particular system. They are, in fact, universal for each generic type of bifurcation, making use of the standard normal forms known from bifurcation theory (see, e.g., [20]). It turns out that the pitchfork and tangent bifurcations occurring for the NPOs in the circular billiard have exactly the same generic features as those of POs, so that we readily can make use of the corresponding uniform approximations which were developed in [16]. That for pitchfork bifurcations will be discussed in section 4.2. Finally, the contribution of the primitive “+” orbit $L_+^{(0)}$ at $r = R$ to the density $\rho(r)$ can be regularized as already stated in [2] and briefly illustrated in section 4.3. All these regularizations will then be used in our numerical calculations in section 5.

We shall only present explicitly the uniform approximations for the density oscillations $\delta\rho(r)$, whereby the basic input is given by the amplitudes $\mathcal{A}_\gamma(r)$ defined in (22), which diverge at the critical points. For symmetry breaking and for bifurcations, the uniform approximations for the kinetic energy densities are then easily obtained according to the semiclassical equations (15) and (16): For $\delta\tau(r)$, we just have to multiply the result of $\delta\rho(r)$ by the factor $p_\lambda^2/2m$. For $\tau_1(r)$, we must furthermore replace the amplitudes $\mathcal{A}_\gamma(r)$ in the resulting expressions for $\delta\rho(r)$ by $\mathcal{A}_\gamma(r)Q_\gamma(r)$. This does, however, not work for the regularization at the boundary $r = R$, as discussed at the end of section 4.3.

4.1. Symmetry breaking at $r = 0$

4.1.1. Linear radial NPOs $L_\pm^{(k)}$. The local regularization for the radial linear orbits $L_\pm^{(k)}$ at $r = 0$ has already been given in [1, 2] and yields the result (25) which is valid for $r \ll R$. Here we first present an alternative derivation of this result, following the perturbative approach of Creagh [15], using r/R as the perturbation parameter which for $r > 0$ breaks the U(1) symmetry. We then follow the approach of [13, 14] to derive a global uniform approximation that is valid up to all distances r for which no new critical phenomenon occurs. (We refer to section 6.3.1 of [4] for an easy understanding of the

main ideas and the technical details.)

The basic idea is that the NPOs $L_{\pm}^{(k)}$ at $r > 0$ can be considered as the result of a symmetry-breaking process. At $r = 0$, they are degenerate, forming a family of orbits with U(1) symmetry obtained by rotation about an angle $\phi \in [0, 2\pi)$. For $r > 0$ this symmetry is broken; the scenario corresponds to the generic case of breaking a U(1) torus into a pair of isolated orbits according to the Poincaré-Birkhoff theorem [20].

We make use of the stationary property of the length function $L_{v,w}(r)$ in (33) at a fixed distance r and for fixed values v, w . With the help of (28) we rewrite it as

$$L_{v,w}(r, \beta) = 2v\sqrt{R^2 - r^2 \sin^2 \beta} + 2r \cos \beta. \quad (59)$$

At the stationary points $\beta_- = 0$ and $\beta_+ = \pi$, this yields exactly the lengths of the orbits $L_{\pm}^{(k)}$ given in (51) with $v = 2k + 1$. For $r = 0$, the function (59) is independent of β and yields the lengths $2(2k + 1)R$ of the degenerate orbit families, in short called “tori”.

We now re-interpret the $L_{v,w}(r, \beta)$ in the following way. We rename the variable β to ϕ and take it as the parameter $\phi \in [0, 2\pi]$ describing the U(1) symmetry of the tori. For $r > 0$, $L_{v,w}(r, \phi)$ yields the lengths of the perturbed tori. To first order in the perturbation parameter r/R , we thus get the actions of the perturbed tori to be

$$S^{(k)}(r, \phi) = S_0^{(k)} + 2rp_{\lambda} \cos \phi, \quad S_0^{(k)} = 2p_{\lambda}(2k + 1)R. \quad (60)$$

According to the classical perturbation theory of Creagh [15], we can now write the contribution of the $L_{\pm}^{(k)}$ orbits to the particle density in (14) as the integral

$$\delta_r \rho(r) = \text{Re} \frac{1}{2\pi} \sum_{k=0}^{\infty} \int_0^{2\pi} \tilde{A}_k(r, \phi) e^{i[S^{(k)}(r, \phi)/\hbar - \mu_0^{(k)} \pi/2 - 3\pi/4]} d\phi, \quad (61)$$

where $\mu_0^{(k)}$ are the Morse indices of the unperturbed tori which will be determined below. The amplitude functions $\tilde{A}_k(r, \phi)$ will also be determined in the following; they must be chosen such that for $r \simeq 0$ the sum of integrals (61) leads to the result (25).

By construction, the *stationary points of* $S^{(k)}(r, \phi)$ at fixed r are $\phi_- = 0$ and $\phi_+ = \pi$ and yield the actions of the isolated $L_{\pm}^{(k)}$ orbits:

$$S^{(k)}(r, \phi_{\pm}) = S_{\pm}^{(k)}(r) = 2p_{\lambda}[(2k + 1)R \mp r]. \quad (62)$$

Hereby ϕ_+ and ϕ_- are the directions into which the orbits start from the point $r > 0$: the “+” orbits start towards $\phi_+ = \pi$, while the “−” orbits start to the opposite direction $\phi_- = 0$. The *stationary-phase approximation* for the integrals (61), with appropriately chosen values of $\tilde{A}_k(r, \phi)$, therefore yields exactly the contributions of the isolated $L_{\pm}^{(k)}$ orbits to (14). Since $S''^{(k)}(r, \phi_+) > 0$ and $S''^{(k)}(r, \phi_-) < 0$, their Morse indices differ by one unit as they must, according to their values given in (58) for small r .

We now take, in a first step, the amplitudes $\tilde{A}_k(r, \phi)$ to be independent of ϕ , using their forms (22) valid for small r , and perform the integral in (61) *exactly* rather than by stationary-phase approximation. This leads to the Bessel function $J_0(2rp_{\lambda}/\hbar)$ with the correct argument, hence reproducing the locally regularized density (25) after summing over all repetitions. This result corresponds to a *local* uniform approximation in the spirit of [12, 15] which is correct locally for $r \simeq 0$ for which the amplitudes were approximated.

(We recall that using the full amplitudes given by (22), the summation over k cannot be done analytically.)

In the second step, required to obtain a *global* uniform approximation valid also for large r , we choose $\tilde{A}_k(r, \phi)$ to be of the form $\tilde{A}_k(r, \phi) = a_k(r) + b_k(r) \cos \phi$. The coefficients $a_k(r)$ and $b_k(r)$ are chosen such that they reproduce the *exact* amplitudes $\mathcal{A}_\pm^{(k)}(r)$ given in (22) at large distances r from the center, where the stationary-phase approximation for the integral is valid. The exact integral for the terms including $b_k(r)$ leads to the Bessel function $J_1(2rp_\lambda)$. As a result, we obtain the following global uniform approximation for the combined contributions of the linear NPOs $L_\pm^{(k)}$ to the particle density oscillations:

$$\delta_r \rho^{(\text{un})}(r) = \sqrt{4\pi r p_\lambda / \hbar} \sum_{k=0}^{\infty} \left\{ \bar{A}_k(r) J_0(2rp_\lambda / \hbar) \cos \left[\frac{1}{\hbar} S_0^{(k)} - \frac{\pi}{2} \mu_0^{(k)} - \frac{3\pi}{4} \right] - \Delta A_k(r) J_1(2rp_\lambda / \hbar) \sin \left[\frac{1}{\hbar} S_0^{(k)} - \frac{\pi}{2} \mu_0^{(k)} - \frac{3\pi}{4} \right] \right\}, \quad (63)$$

where

$$\bar{A}_k(r) = \frac{1}{2} \left[\mathcal{A}_+^{(k)}(r) + \mathcal{A}_-^{(k)}(r) \right], \quad \Delta A(r) = \frac{1}{2} \left[\mathcal{A}_-^{(k)}(r) - \mathcal{A}_+^{(k)}(r) \right]. \quad (64)$$

Hereby $\mathcal{A}_\pm^{(k)}(r)$ are the exact amplitudes obtained from (22) (we have omitted the Fermi energy $\tilde{\lambda}$ in their arguments), using the properties of the orbits $L_\pm^{(k)}$ given in section 3.5.

The result (63) is finite at $r = 0$, where the second term $\propto J_1(2rp_\lambda)$ does not contribute. This term becomes important, however, at larger distances r . When $2rp_\lambda \gg \hbar$, we may use the asymptotic forms of the Bessel functions for large arguments [21] (which is tantamount to using the stationary-phase approximation for the above integrals), and then the result (63) goes over into the contributions of the isolated $L_\pm^{(k)}$ orbits corresponding to (14)

$$\delta_r \rho^{(\text{un})}(r) \longrightarrow \sum_{k=0}^{\infty} \mathcal{A}_+^{(k)}(r) \cos \left[\frac{1}{\hbar} S_+^{(k)}(r) - \frac{\pi}{2} (\mu_0^{(k)} - 1/2) - \frac{3\pi}{4} \right] + \sum_{k=0}^{\infty} \mathcal{A}_-^{(k)}(r) \cos \left[\frac{1}{\hbar} S_-^{(k)}(r) - \frac{\pi}{2} (\mu_0^{(k)} + 1/2) - \frac{3\pi}{4} \right]. \quad (65)$$

In order to obtain the correct Morse indices (58) (valid below the bifurcation points r_k of the “+” orbits), we now see that we have to choose $\mu_0^{(k)} = 6k + 5/2$, which corresponds to the average value of $\mu_+^{(k)}$ and $\mu_-^{(k)}$. With this, the phases can be simplified to a common sign factor and the result (63) becomes

$$\delta_r \rho^{(\text{un})}(r) = \sqrt{4\pi r p_\lambda / \hbar} \sum_{k=0}^{\infty} (-1)^k \left\{ \bar{A}_k(r) J_0(2rp_\lambda / \hbar) \cos[S_0^{(k)} / \hbar] - \Delta A_k(r) J_1(2rp_\lambda / \hbar) \sin[S_0^{(k)} / \hbar] \right\}. \quad (66)$$

The result (66) can only be used below the critical points $r_k = R/(2k + 1)$ at which the “+” orbits with $k > 1$ bifurcate, or below the boundary $r = R$ where the amplitude for the primitive “+” orbit with $k = 0$ diverges. Near these critical points, we need different uniform approximations that will be discussed in sections 4.2 and 4.3.

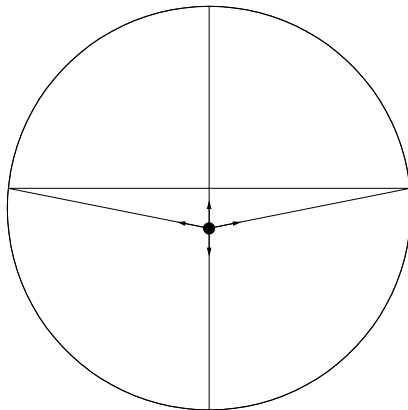


Figure 8. Non-linear NPO (2,1) (triangle, in the text called ∇) starting from a point r (black dot) near the center, where it was created from the PO (2,1) (vertical diameter) by U(1) symmetry breaking. The arrows indicate the starting directions of the four isolated orbits (see text for details).

4.1.2. *Non-linear NPOs* $(2k, k)$. The non-linear NPOs with $(v, w) = (2k, k)$ and $k = 1, 2, \dots$ are created from the k -th repetitions $(2k, k)$ of the diametrical PO by symmetry breaking at $r = 0$ (see the systematics in section 3.6). For small r , they leave their starting points r perpendicular to the diameter containing the POs $(2k, k)$. As an example, we show in figure 8 the NPO (2,1), which we here call ∇ , with a starting point r (black dot) close to the center. For $r = 0$, these NPOs are degenerate with the families of diametrical POs and their semiclassical amplitudes diverge. The uniform approximation for these NPOs can be derived in a similar way as above for the linear NPOs. We first give the derivation for the orbit ∇ (whose analytical properties are given in the appendix) and then generalize the result to all NPOs $(2k, k)$. For $r = 0$, the PO orbit family (2, 1) has the action $S_{1r} = 4p_\lambda R$. For $r > 0$, the family breaks up into a degenerate pair of isolated diametrical POs, starting in opposite directions along the diameter going through r (this is the vertical diameter in figure 8), plus a discrete pair of NPOs ∇ related by time-reversal symmetry (cf. the triangle in the figure, starting in the two directions indicated by the arrows). Their action is $S_2(r) = p_\lambda L_{2,1}(r)$ with the length $L_{2,1}(r)$ given in (A.3). We can obtain the actions of all four isolated orbits from the stationary points of the action function

$$S_2(r, \phi) = S_{1r} + 2\Delta\tilde{S}(r) \sin^2\phi, \quad \Delta\tilde{S}(r) = r^2 p_\lambda / R. \quad (67)$$

At $\phi = 0$ and π , it yields the action S_{1r} of the diameter orbit, and at $\phi_\pm = \pm\pi/2$, it yields the perturbed action $S_{1r} + 2\Delta\tilde{S}(r)$ of the ∇ orbit, valid for small r as given in (A.5). Note that the values of ϕ at these stationary points correspond to the directions (shown by the arrows in figure 8) in which the perturbed isolated orbits leave the point r (for the ∇ orbits only in the limit $r \rightarrow 0$ where the symmetry breaking occurs).

We thus write the common uniform contribution of the four perturbed isolated orbits to the particle density (14) as the following integral:

$$\delta\rho_{2,1}(r) = \text{Re} \frac{1}{2\pi} \int_{-\pi}^{+\pi} \tilde{A}(r, \phi) e^{i[S_2(r, \phi)/\hbar - \mu_0\pi/2 - 3\pi/4]} d\phi. \quad (68)$$

For a constant amplitude $\tilde{A}(r, \phi)$ independent of ϕ , the integral in (68) yields the Bessel function $J_0(\Delta\tilde{S}(r)/\hbar)$, corresponding to a local uniform approximation valid near $r = 0$. Adding to $\tilde{A}(r, \phi)$ a term proportional to $\sin^2\phi$ yields an additional Bessel function J_1 with the same argument. Proceeding like above for the linear NPOs and replacing the perturbative action change $\Delta\tilde{S}(r)$ in the arguments of the Bessel functions by the exact difference $\Delta S(r)$ given in (71) below, we find the global uniform approximation for the combined NPOs and POs (2,1) to be

$$\begin{aligned} \delta\rho_{2,1}^{(\text{un})}(r) = \sqrt{\frac{2\pi\Delta S(r)}{\hbar}} \left\{ \bar{A}(r) J_0\left(\frac{\Delta S(r)}{\hbar}\right) \cos\left[\frac{1}{\hbar}\bar{S}(r) - \frac{\pi}{2}\mu_0 - \frac{3\pi}{4}\right] \right. \\ \left. + \Delta A(r) J_1\left(\frac{\Delta S(r)}{\hbar}\right) \sin\left[\frac{1}{\hbar}\bar{S}(r) - \frac{\pi}{2}\mu_0 - \frac{3\pi}{4}\right] \right\}. \quad (69) \end{aligned}$$

The amplitudes above are given by

$$\bar{A}(r) = \frac{1}{2} [\mathcal{A}_{1r}(r) + \mathcal{A}_{2,1}(r)], \quad \Delta A(r) = \frac{1}{2} [\mathcal{A}_{1r}(r) - \mathcal{A}_{2,1}(r)], \quad (70)$$

where $\mathcal{A}_{1r}(r)$ is the amplitude (22) evaluated for the diameter PO (2,1) in term of its properties given in section 3.4 and $\mathcal{A}_{2,1}(r)$ that of the ∇ orbit using its exact properties given in (A.3), (A.4). Both amplitudes must include a discrete degeneracy factor 2 corresponding to their two starting directions. Furthermore, the quantities $\Delta S(r)$ and $\bar{S}(r)$ are defined by

$$\Delta S(r) = \frac{1}{2} [S_{2,1}(r) - S_{1r}], \quad \bar{S}(r) = \frac{1}{2} [S_{2,1}(r) + S_{1r}], \quad (71)$$

where $S_{2,1}(r)$ is the *exact* action of the ∇ orbit, given by $S_{2,1}(r) = p_\lambda L_{2,1}(r)$ using (A.3).

For large enough distances r such that $\Delta S(r) \gg \hbar$, we can use the asymptotic forms of the Bessel functions for large arguments, and (69) goes over into the sum of the contributions of the isolated diameter POs and ∇ orbits

$$\begin{aligned} \delta\rho_2^{(\text{un})}(r) \longrightarrow A_{1r}(r) \cos\left[\frac{1}{\hbar}S_{1r} - \frac{\pi}{2}(\mu_0 - 1/2) - 3\pi/4\right] \\ + A_2(r) \cos\left[\frac{1}{\hbar}S_{2,1}(r) - \frac{\pi}{2}(\mu_0 + 1/2) - 3\pi/4\right]. \quad (72) \end{aligned}$$

With the choice $\mu_0 = 11/2$, we obtain the correct Morse indices $\mu_{1r} = 5$ for the diameter orbit and $\mu_{2,1} = 6$ for the ∇ orbit.

The uniform result (69) gives a finite combined contribution of the degenerate orbit families at $r = 0$. Since the orbit ∇ undergoes no bifurcation and its amplitude stays finite for all $r > 0$, the uniform result (69) is valid in the entire region $0 \leq r \leq R$.

The result (69) looks very similar to the uniform contribution (66) of the linear NPOs, except that the argument of the Bessel functions here is quadratic in r (for small

r), which yields a slower departure from its maximum. This is characteristic of the long-ranged irregular oscillations $\delta_{\text{irr}}\rho(r)$ that are due to non-linear NPOs. In fact, the presently discussed class of non-linear NPOs $(2k, k)$ is dominating the irregular part of the density oscillations near $r = 0$, as we shall see in section 5.

We therefore now generalize (69) to include all NPOs of type $(2k, k)$ that are created by symmetry breaking at $r = 0$ from the k -fold repetitions of the periodic diameter orbit (2,1). For that we simply have to substitute the amplitudes $\mathcal{A}_{2,1}(r)$ and actions $S_{2,1}(r)$ in the equations (70), (71) by those obtained from the general formulae (33) and (40) for the NPOs with $(v, w) = (2k, k)$, and the quantities $\mathcal{A}_{1r}(r)$ and S_{1r} by those obtained from (47) and (49) for the POs. The Morse index in (69) must be substituted by $\mu_0^{(k)} = 6k - 1/2$. After these substitutions we must, of course, sum over all $k > 0$. Taking out a common phase factor, we obtain the global uniform approximation for the dominating contribution to the irregular density oscillations:

$$\delta_{\text{irr}}\rho^{(\text{un})}(r) = \sum_{k=1}^{\infty} \sqrt{\frac{2\pi\Delta S_k(r)}{\hbar}} (-1)^k \left\{ \bar{A}_k(r) J_0\left(\frac{\Delta S_k(r)}{\hbar}\right) \cos\left[\frac{1}{\hbar}\bar{S}_k(r) + \frac{\pi}{4}\right] + \Delta A_k(r) J_1\left(\frac{\Delta S_k(r)}{\hbar}\right) \sin\left[\frac{1}{\hbar}\bar{S}_k(r) + \frac{\pi}{4}\right] \right\}, \quad (73)$$

where the amplitudes are

$$\bar{A}_k(r) = \frac{1}{2} [\mathcal{A}_{kr}(r) + \mathcal{A}_{2k,k}(r)], \quad \Delta A_k(r) = \frac{1}{2} [\mathcal{A}_{kr}(r) - \mathcal{A}_{2k,k}(r)], \quad (74)$$

and the action functions are

$$\Delta S_k(r) = \frac{1}{2} [S_{2k,k}(r) - S_{kr}], \quad \bar{S}_k(r) = \frac{1}{2} [S_{2k,k}(r) + S_{kr}], \quad S_{kr} = 4kp_{\lambda}R. \quad (75)$$

The subscripts “ kr ” refer to the diametrical POs with their properties given in section 3.4, and the subscripts “ $2k, k$ ” to the NPOs with their properties given in section 3.3.

The NPOs $(2k, k)$ exist at all $r > 0$ and undergo no bifurcations. The uniform result (73) is therefore valid in the whole range $r \in [0, R]$. In the numerical calculations presented in section 5, it will be seen that the summation over k can be practically limited to $k_{\text{max}} \sim 10 - 20$ in all cases.

4.2. Uniform approximations for bifurcations

Here we discuss the uniform approximations needed to regularize the divergences of the semiclassical amplitudes arising at bifurcations of the closed orbits. To our knowledge, there exists no systematic study and classification of bifurcations of *non-periodic* closed orbits in the literature. We therefore had to convince ourselves that the bifurcations occurring in our present system are of the same generic types as those known [20, 22] for periodic orbits. This appears, indeed, to be the case. For the pitchfork bifurcations, we shall demonstrate this in a particular example in section 4.2.1 and then present the corresponding uniform approximation for the semiclassical particle density. In section 4.2.2 we briefly discuss the tangent bifurcations.

4.2.1. *Pitchfork bifurcations.* In the left panels of figure 2 we have shown two successive pitchfork bifurcations. We shall take the example at the critical radius $r = R/3$ where the non-linear orbit Λ (3,1) is created from the linear orbit $L_+^{(1)}$. We draw particular attention to the bifurcation diagram on the lower left of figure 2. For isolated periodic orbits of $D = 2$ dimensional systems, the corresponding diagrams are obtained when the trace of the stability matrix, $\text{Tr } M(\epsilon)$ as function of a bifurcation parameter ϵ , is considered. We assume a bifurcation to occur at the point $\epsilon = 0$. In the trace formula for the level density of such systems [3], the quantity $\text{Tr } M(\epsilon) - 2$ appears under a root in the denominator of the semiclassical amplitudes, which diverge at the bifurcation point where $\text{Tr } M(0) = 2$. Now, it is a characteristic feature [16, 18] of a generic pitchfork bifurcation that the slopes of the functions $\text{Tr } M(\epsilon)$ of the two orbits involved in the bifurcation fulfill the following relation at the bifurcation point:

$$\text{Tr } M'_B(0) = -2 \text{Tr } M'_A(0). \quad (76)$$

Hereby A is the parent orbit which changes its stability at the bifurcation point and B the daughter orbit that is created at the bifurcation and only exists on one side of it. (For a mathematical proof of this ‘‘slope theorem’’, we refer to [23].)

In our present system, the decisive quantity under a root in the denominator of the semiclassical amplitudes (22) is the Jacobian $\mathcal{J}_{v,w}(r)$, and r is the bifurcation parameter. In the example of figure 2 under discussion, $L_+^{(1)}$ is the parent orbit A and Λ is the daughter orbit B existing only above the bifurcation point $r = R/3$. Using the explicit results (52) and (A.10) for the Jacobians of these two orbits, we find

$$\left. \frac{d}{dr} \mathcal{J}_{3,1}(r) \right|_{r=R/3} = -\frac{4}{p\lambda}, \quad \left. \frac{d}{dr} \mathcal{J}_+^{(1)}(r) \right|_{r=R/3} = \frac{2}{p\lambda}, \quad (77)$$

so that the slope theorem (76) is, indeed, satisfied.

A pitchfork bifurcation which is generic in the sense of Meyer [22] is period-doubling: the new orbit B has twice the period of the parent orbit A at the bifurcation point. However, in systems with discrete symmetries the pitchfork bifurcations are typically isochronous [18, 24, 25]: both orbits have the same periods at the bifurcation point, but the daughter orbit B has a double discrete degeneracy compared to the parent orbit A. For the NPOs discussed here, the pitchfork bifurcation is of the second, non-generic type: their running times $T(r, \tilde{\lambda})$ (given here simply by their lengths) are identical at the bifurcation point, but the Λ orbit has a degeneracy of two due its time-reversal symmetry while the $L_+^{(1)}$ orbit is not degenerate.

Finally, the following rule is known [16] for the Maslov index appearing in the trace formula: at the pitchfork bifurcation, the index of the parent orbit A changes by one unit, and the index of the orbit B existing after the bifurcation is the same as that of the orbit A before the bifurcation. Using our results in section 3.5 and the appendix, we see that this rule is, indeed, also fulfilled here by the Morse indices: the Morse index of the $L_+^{(1)}$ orbit changes from 8 to 7 at $r = R/3$, and the Λ orbit has the Morse index 8 close to $r > R/3$. After these affirmations of the nature of the present pitchfork bifurcation, we can immediately apply the uniform approximation that was developed

in [16] to obtain the following common contribution of the $L_+^{(1)}$ and Λ orbits to the particle density oscillations in terms of Bessel functions of non-integer orders:||

$$\begin{aligned} \delta\rho_{\text{pb}}^{(\text{un})}(r) &= \text{Re} \sqrt{\frac{\pi\Delta S(r)}{2\hbar}} e^{i[\bar{S}(r)/\hbar - \pi\mu_0/2 - \pi]} \\ &\times \left\{ \bar{A}(r) \left[\sigma_0 J_{1/4} \left(\frac{\Delta S(r)}{\hbar} \right) e^{i\sigma_1\pi/8} + J_{-1/4} \left(\frac{\Delta S(r)}{\hbar} \right) e^{-i\sigma_1\pi/8} \right] \right. \\ &\left. + \Delta A(r) \left[J_{3/4} \left(\frac{\Delta S(r)}{\hbar} \right) e^{i3\sigma_1\pi/8} + \sigma_0 J_{-3/4} \left(\frac{\Delta S(r)}{\hbar} \right) e^{-i3\sigma_1\pi/8} \right] \right\}, \end{aligned} \quad (78)$$

with

$$\begin{aligned} \bar{A}(r) &= \left[\frac{\mathcal{A}_{3,1}(r)}{2} + \frac{\mathcal{A}_+^{(1)}(r)}{\sqrt{2}} \right], & \Delta A(r) &= \left[\frac{\mathcal{A}_{3,1}(r)}{2} - \frac{\mathcal{A}_+^{(1)}(r)}{\sqrt{2}} \right], \\ \bar{S}(r) &= \frac{1}{2} [S_{3,1}(r) + S_+^{(1)}(r)], & \Delta S(r) &= \frac{1}{2} [S_{3,1}(r) - S_+^{(1)}(r)], \\ \sigma_0 &= \text{sign}(r - R/3), & \sigma_1 &= \text{sign}(\Delta S), \end{aligned} \quad (79)$$

in terms of the exact amplitudes $\mathcal{A}_{3,1}(r)$, $\mathcal{A}_+^{(1)}(r)$ and actions $S_{3,1}(r)$, $S_+^{(1)}(r)$ of the Λ and $L_+^{(1)}$ orbits, respectively. The choice of $\mu_0 = 7$ yields the correct Morse indices of the isolated orbits on either side of the bifurcation. Note that for $r < R/3$, there exists an imaginary ‘‘ghost’’ orbit Λ which contributes with real action $S_{3,1}(r)$ and amplitude $\mathcal{A}_{3,1}(r)$ which are just the analytical continuations of these properties of the real Λ orbit, as given in (A.8) and (A.10). Note also that the amplitude $\mathcal{A}_{3,1}$ must include the degeneracy factor 2 due to the two time orientations of the Λ orbit.

At the bifurcation point, the result (78) takes the finite value

$$\delta\rho_{\text{pb}}^{(\text{un}2)}(R/3) = \frac{1}{\hbar^{3/4}} \frac{9p_\lambda^{3/4}\Gamma(1/4)}{32\pi^2 R^{5/4}} \cos\left(\frac{16Rp_\lambda}{3\hbar} - \frac{5\pi}{8}\right). \quad (80)$$

The uniform approximation (78) is again global in the sense that it goes over into the sum of the isolated contributions of both orbits (including the degeneracy of the Λ orbit) sufficiently far away from the bifurcation, where the argument of the Bessel functions is large enough so that their asymptotic forms can be used.

Having confirmed that all other pitchfork bifurcations occurring in the circular billiard are of the same type, we can apply the result (78) to them, replacing in (79) the amplitudes and actions of the $L_+^{(1)}$ orbit by those of the parent orbit, those of the Λ orbit by those of the daughter orbit (irrespective of whether this is a NPO or a PO like in the other pitchfork bifurcations seen in figure 2), and σ_0 by $\text{sign}(r - r_b)$ using the appropriate bifurcation radius r_b . The Morse index μ_0 in (78) has to be chosen according the rules given in [16].

|| We can also derive this result by making an ansatz similar to (68) and expanding the action function $S_{3,1}(r, \beta) = p_\lambda L_{3,1}(r, \beta)$ using (A.8) in the phase of the integrand around the stationary point $r = R/3$, $\beta = \pi$. Expanding it up to first order in $\epsilon = r - R/3$ and fourth order in $\delta = \beta - \pi$, we obtain exactly the (one-dimensional) normal form of the action for the pitchfork bifurcation that was used in [16] to derive the uniform approximation

We must emphasize that the uniform approximation (78) only holds up to distances from the bifurcation point r , until which the respective orbits do not change their nature by a new bifurcation (or by symmetry restoring when going towards $r = 0$). This becomes a practical problem when successive bifurcations lie close, i.e., when the relevant action difference between the two points is of the order of, or smaller than \hbar . We discuss this problem again in the following section and in section 5.

4.2.2. Tangent bifurcations. The tangent bifurcations of POs in systems with $D = 2$ always occur as generic isochronous bifurcations [22, 24]. The two orbits created thereby have infinite slopes of their stability traces [16, 23]:

$$\lim_{\epsilon \rightarrow 0} \text{Tr } M'(\epsilon) = \pm\infty. \quad (81)$$

The same holds for the Jacobians of the NPOs created by tangent bifurcations in our present system, as seen for the example of the orbits P and P' on the right side of figure 2. Characteristically, too, the Morse indices of the two orbits differ by one unit close to the bifurcation (i.e., before any further bifurcation occurs).

The global uniform approximation for the tangent bifurcation has been derived in [16]; it looks similar to (78) except that the Bessel functions have the orders $\pm 1/3$ and $\pm 4/3$ (and can also be expressed in terms of Airy functions, cf. also [18]; on that side of the bifurcation where the orbits are not real, modified Bessel functions occur).

The reason for not quoting the result of [16] here is that for all NPOs in the circular billiard created in this way, the tangent bifurcation occurring at the critical point $r = r_{v,w}$ is immediately followed by a pitchfork bifurcation of one of the orbits at a nearby critical point $r = r_{v,w}^{\text{PO}} > r = r_{v,w}$ where the PO (v, w) is created (see the systematics in section 3.6). The two bifurcations lie close in the sense that the action difference $S_{v,w}(r = r_{v,w}^{\text{PO}}) - S_{v,w}(r = r_{v,w})$ is *not* much larger than \hbar . Consequently, the arguments of the Bessel functions in the uniform approximations are never large enough to allow for their asymptotic expansion. In other words: in the region between the two bifurcations, the two orbits are never sufficiently isolated for the two bifurcations to be treated separately. This necessitates to treat what in the relevant literature is called a ‘‘codimension-two’’ bifurcation. Such bifurcations have been investigated and semiclassically applied in [26, 27]. We have, however, not been able to find an appropriate uniform approximation for our present bifurcation scenario which is similar to, but not identical with the ‘‘butterfly catastrophe’’ discussed in [26]. Luckily, the NPOs created by tangent bifurcations are practically negligible (cf. end of section 5.1).

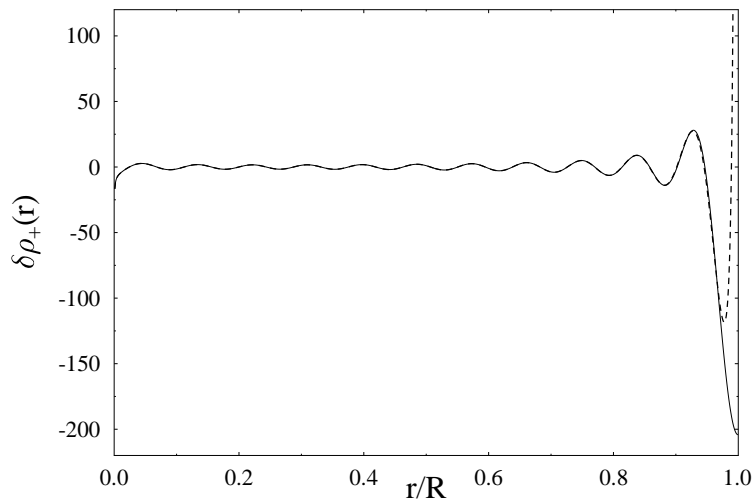


Figure 9. Contribution of primitive $L_+^{(0)}$ orbit to the particle density in the circular billiard with $N = 606$ particles ($\hbar^2/2m = R = 1$). *Solid line:* uniform approximation (82), *dashed line:* asymptotic expression (83).

4.3. Regularization at the boundary $r = R$

We have already mentioned in section 3.3 that the semiclassical amplitude of the orbit $L_+^{(0)}$, which is responsible for the Friedel oscillations [2], diverges at the boundary $r = R$ due to the zero of its Jacobian (52). A method to regularize this divergence for the density using a uniform approximation of the Green function for short times was proposed in [28]. The specific result for a two-dimensional billiard was given in [2]. For the circular billiard we obtain the following uniform approximation for the contribution of the primitive “+” orbit $L_+^{(0)}$ to the particle density:

$$\delta\rho_+^{(\text{un})}(r) = -\frac{p_\lambda}{2\pi\hbar} \sqrt{\frac{R}{r}} \frac{J_1[2(R-r)p_\lambda/\hbar]}{(R-r)}. \quad (82)$$

Sufficiently far from the boundary, this result goes over into the correct expression for the isolated $L_+^{(0)}$ orbit using (22) and its properties given in (62), (52):

$$\delta\rho_+^{(\text{un})}(r) \longrightarrow -\frac{1}{2\pi(R-r)} \sqrt{\frac{p_\lambda R}{\pi\hbar r(R-r)}} \cos\left[\frac{1}{\hbar} S_+^{(0)}(r) - \frac{3}{4}\pi\right]. \quad (83)$$

This is illustrated in figure 9. The “recovery distance” d from the boundary, at which the diverging asymptotic result goes over into the uniform result, is bounded from below by the Fermi wave length:

$$d \gtrsim \hbar/p_\lambda. \quad (84)$$

For the particle number $N = 606$ with $p_\lambda = 35.8186$ chosen here, this corresponds to $d \gtrsim 0.03$.

Unfortunately, we have not been able to derive corresponding uniform results for the kinetic energy densities. [Note also that the relations (23) and (26) do not hold at and near the boundary $r = R$.]

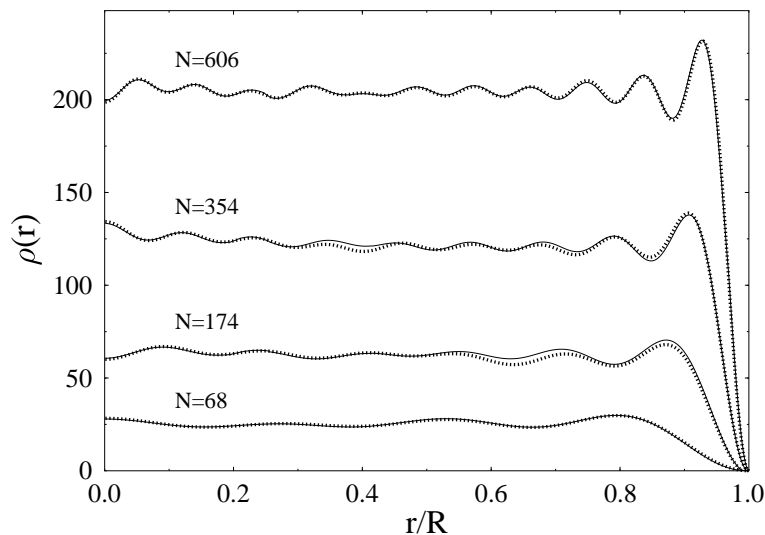


Figure 10. Particle density in the two-dimensional disk billiard with $N = 606, 354, 174$ and 68 particles (units: $\hbar^2/2m = R = 1$). The dotted lines are the quantum results, the solid lines the converged semiclassical results using the number of orbits and the regularizations discussed in the text.

5. Numerical results for density oscillations

In this section we present numerical calculations for the spatial densities in the circle billiard and compare our semiclassical results with exact quantum-mechanical results. In section 5.1 we will discuss the convergence of the sum over closed orbits in semiclassical expressions (14) – (16), and in section 5.2 we address the role of closed main shells and investigate the relation of the spatial density oscillations with the shell effects in the total energy of the system.

5.1. Convergence of orbit sums

Figure 10 shows the total particle density $\rho(r)$ for four values of the number of N particles bound in the circular billiard. The dotted line is the quantum result (1), and the solid line the converged semiclassical result obtained as explained below. The numbers $N = 606$ and 68 correspond to filled main shells (“closed-shell systems”) and the numbers $N = 354$ and 174 to half-filled main shells (“mid-shell systems”); we refer to the discussion of the shell structure in section 5.2 (cf. figure 14). The agreement for the closed-shell systems is excellent, that for the mid-shell systems is also very satisfactory.

In figure 11 we show how the convergence of the semiclassical result for $N = 606$ comes about; here only the oscillating part $\delta\rho(r)$ of the density is shown. Dotted lines show the quantum results, identical in all panels, and solid lines the semiclassical results in various approximations. From bottom to top, an increasing number of closed orbits is included in the sum (14). In the three lowest panels, the amplitudes \mathcal{A}_γ (22) for isolated orbits are used; in the top panel, the uniform approximations for the symmetry

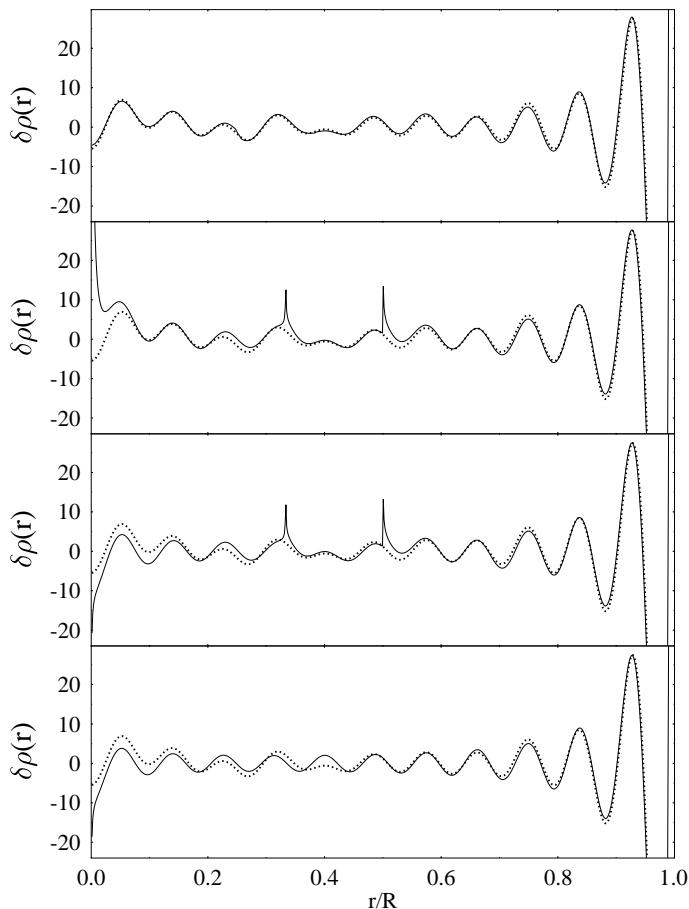


Figure 11. Oscillating part $\delta\rho(r)$ of the particle density for $N = 606$ particles like in figure 10. *Dots*: quantum results (identical in all panels). *Solid lines*: semiclassical results; in the three lowest panels as isolated orbits with amplitudes (22), and in the top panel using the uniform approximations (66), (73) and (78) (see text for details).

breaking at $r = 0$ and for the pitchfork bifurcations are used.

In the bottom panel, only the primitive linear NPOs $L_{\pm}^{(k=0)}$ are included. In spite of their weak divergence at $r = 0$, their contribution already accounts for most of the density oscillations. In particular, the Friedel oscillations are well reproduced by the “+” orbit up to the highest peak; only close to the boundary its contribution diverges (cf. the contribution of the “+” orbit alone in figure 9). In the second panel from below, the linear orbits $L_{\pm}^{(k=1)}$ have been added, together with the non-linear orbit $\Lambda(3,1)$ and the triangle PO $(3,1)$ emerging from $L_{+}^{(k=1)}$ by pitchfork bifurcations at $r = R/3$ and $r = R/2$, as shown in figure 2 (left panels). The agreement with the quantum results is slightly improved in the region $0.3 \lesssim r/R \lesssim 0.6$, but at the cost of the divergences at the two bifurcation points. In the third panel, we have furthermore added the non-linear orbit $\nabla(2,1)$ and the diameter PO $(2,1)$. This improves the agreement around $0.1 \lesssim r/R \lesssim 0.2$, but at the cost of a stronger divergence at $r = 0$. In the top panel, finally, we have used the uniform approximation (66) for the symmetry breaking at $r = 0$ of the “+” and “-” orbits, including also the linear orbits $L_{\pm}^{(k=2)}$ and the orbits $(2k+1, k)$

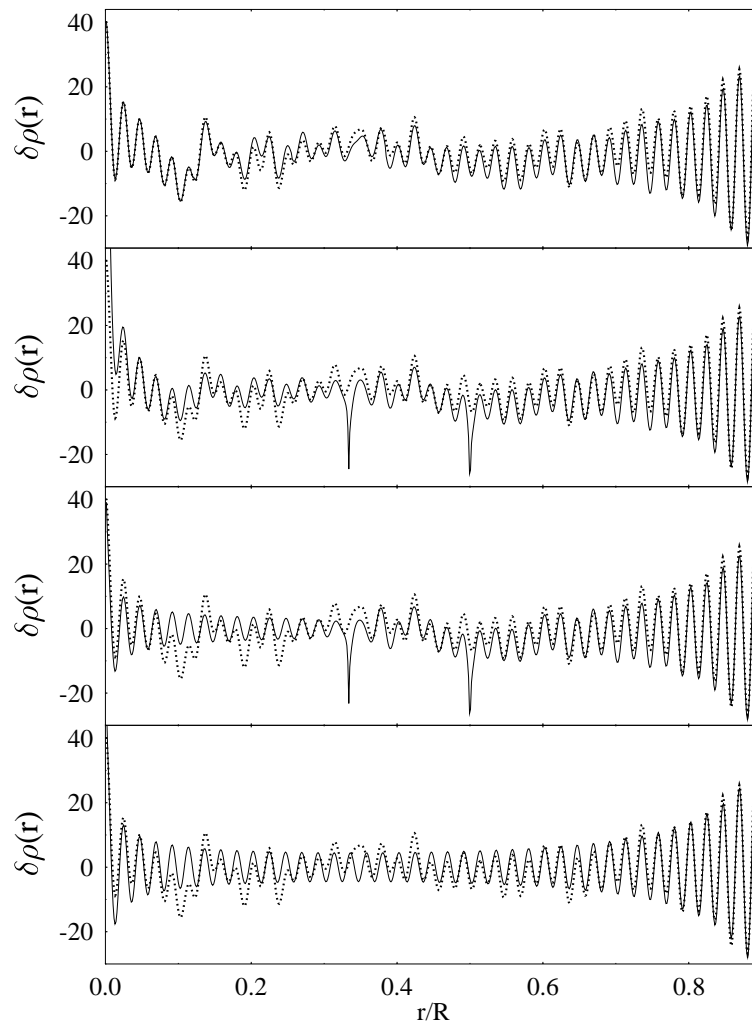


Figure 12. Same as figure 11, but for $N = 9834$ particles.

bifurcating from them, the uniform approximation (78) for the pitchfork bifurcations of the NPOs and POs (3,1) and (5,2), and finally the uniform approximation (73) for the symmetry breaking at $r = 0$ of the NPOs and POs $(2k, k)$ including values of k up to $k = 10$. The agreement with quantum mechanics is now excellent, except very close to the boundary where the isolated “+” orbit (with $k = 0$) diverges. Employing the regularization at $r = R$ discussed in section 4.3 and shown separately in figure 9 leads to the result shown in figure 10.

The same analysis is made in figure 12 for a larger system with $N = 9834$ particles; the convergence is similar as above. Here the irregular part of the oscillations is seen to be well reproduced by the contributions of the nonlinear NPOs $(2k, k)$ in the two upper panels. We have omitted the surface region $r \geq 0.9R$ because the peaks of the last Friedel oscillations are so high that the oscillations in the interior would not be recognizable on their scale. The contribution of the primitive “+” orbit alone, however, reproduces the quantum density almost exactly for $r > 0.9R$ like in figure 10.

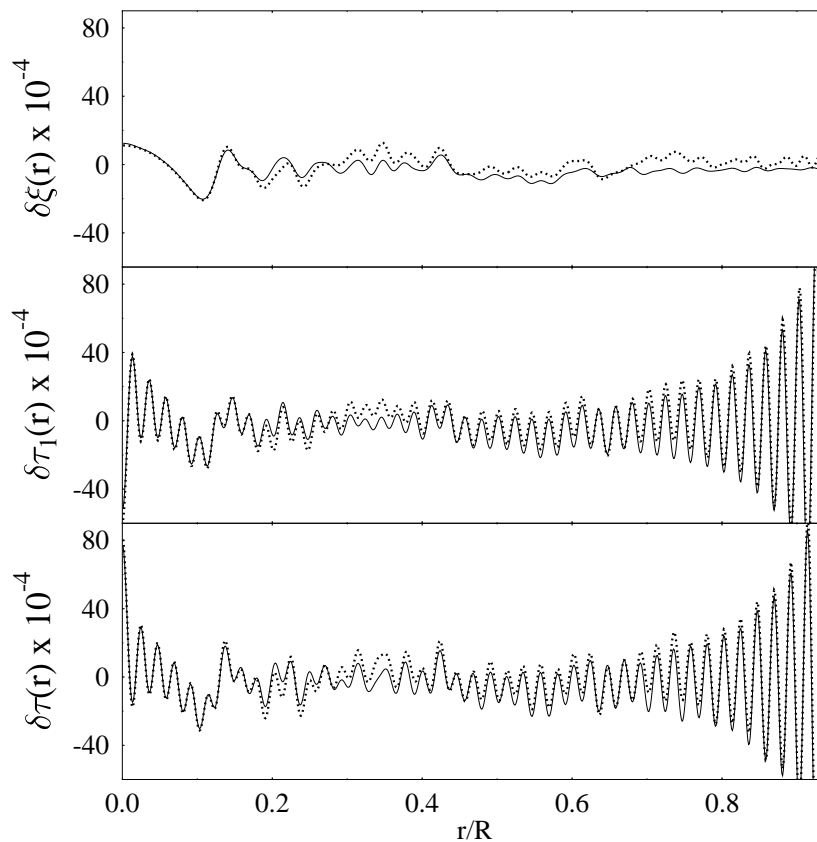


Figure 13. Quantum-mechanical results (dots) and uniform semiclassical results (lines) for $N = 9834$ particles as in top panel of figure 12, but for the oscillating parts of the kinetic energy densities $\delta\xi(r)$ (top panel), $\delta\tau_1(r)$ (center panel), and $\delta\tau(r)$ (bottom panel).

In figure 13 we show the oscillating parts of the kinetic energy densities of the system with $N = 9834$ particles using the same orbits and uniform approximations as in the top panel of figure 12. Like there, the agreement is best in the region $0 \leq r \lesssim 0.2R$, where the rapid oscillations are dominated by the linear orbits $L_{\pm}^{(k)}$ and the slow, irregular oscillations by the orbits $(2k, k)$. We see that the rapid oscillations are opposite in phase in the two kinetic energy densities $\delta\tau(r)$ and $\delta\tau_1(r)$, as expressed in the relation (26) which is due to the fact that the momentum mismatch for all linear orbits has the constant value $Q = -1$. The rapid oscillations cancel therefore in the quantity $\delta\xi(r)$, seen in the top panel of figure 13, which is due exclusively to the nonlinear orbits (except very close to the boundary) as discussed in general in [1].

The small discrepancies at $r \gtrsim 0.2R$ are due to missing longer orbits in the sums contributing to (14) – (16). In principle, these can be included using the general formulae given in section 2. There is a practical problem, however. With increasing values of k , the bifurcations tend to lie denser along the radial variable r . The uniform approximations given in section 4, including those for the symmetry breaking at $r = 0$, can only be used for the regularization of a divergence around one critical point at a time. It is necessary that, while going away from one critical point, an

asymptotic domain be reached in which the uniform approximation becomes identical to the sum of contributions of the isolated orbits, before one approaches the next critical point. Midways between the two critical points, one can then switch from one uniform approximation to the next one. This is what we have done in the examples given in the figures of this section; it was possible with the limitation of $k_{\max} = 2$ for the bifurcating orbits of type $(2k + 1, k)$. For longer orbits, successive bifurcations lie so close that their actions at the two bifurcation points differ by less than $\sim \hbar$ and hence the bifurcations cannot be treated separately. This is the same problem as arises for the pairs of orbits created by tangent bifurcations (see e.g. figure 2, right panels), as discussed in section 4.2.2. We can consider it as a lucky circumstance that, with the quality of the semiclassical approximation reached in the above figures, all those longer orbits can be practically neglected.

5.2. Relation to shell effects in the total energy

As already observed in figure 10, the quality of the semiclassical approximation depends to some extent on the shell situation of the system with N particles. This is known also from semiclassical calculations of the total energy of finite fermionic systems [29, 30, 31]. To study the shell structure, it is instructive to consider the *shell-correction energy* δE_{tot} defined [32] as the oscillating part of the total energy:

$$\delta E_{\text{tot}} = 2 \sum_{E_j \leq \lambda} E_j - 2 \int_0^{\tilde{\lambda}} E \tilde{g}(E) \mathbb{E} = 2 \int_0^{\lambda} E g(E) \mathbb{E} - 2 \int_0^{\tilde{\lambda}} E \tilde{g}(E) \mathbb{E}. \quad (85)$$

Here $g(E) = \sum_j \delta(E - E_j)$ is the exact level density and $\tilde{g}(E)$ its average part. λ and $\tilde{\lambda}$ are the Fermi energies determined by $N = \mathcal{N}(\lambda) = \tilde{\mathcal{N}}(\tilde{\lambda})$ in terms of the “number counting functions”, which are defined as the first integrals of the two level densities:

$$\begin{aligned} \mathcal{N}(E) &= 2 \sum_j \Theta(E - E_j) = 2 \int_0^E g(E) \mathbb{E}, \\ \tilde{\mathcal{N}}(E) &= 2 \int_0^E \tilde{g}(E) \mathbb{E} = \frac{E}{2E_0} - \sqrt{\frac{E}{E_0}} + \frac{1}{3} + \mathcal{O}(E^{-1/2}). \end{aligned} \quad (86)$$

The explicit expression for $\tilde{\mathcal{N}}(E)$ is obtained from the Weyl expansion [7, 8]. In figure 14 we show the shell-correction energy as a function of the particle number N in the region $0 \leq N \leq 650$. A very pronounced shell structure is seen. The minima of $\delta E_{\text{tot}}(N)$ correspond to closed “main shells” for which the level density at the Fermi energy has a minimum, too, corresponding to a low degeneracy of the spectrum. These main shells may be counted by the number M appearing in (25). The maxima of $\delta E_{\text{tot}}(N)$ correspond to regions of high degeneracy for “mid-shell” systems. This behavior of the energy shell structure has been studied extensively, e.g., in nuclei [33].

In order to calculate the shell-correction energy δE_{tot} semiclassically, it is convenient to express it directly in terms of the oscillating part $\delta g(E) = g(E) - \tilde{g}(E)$ of the level

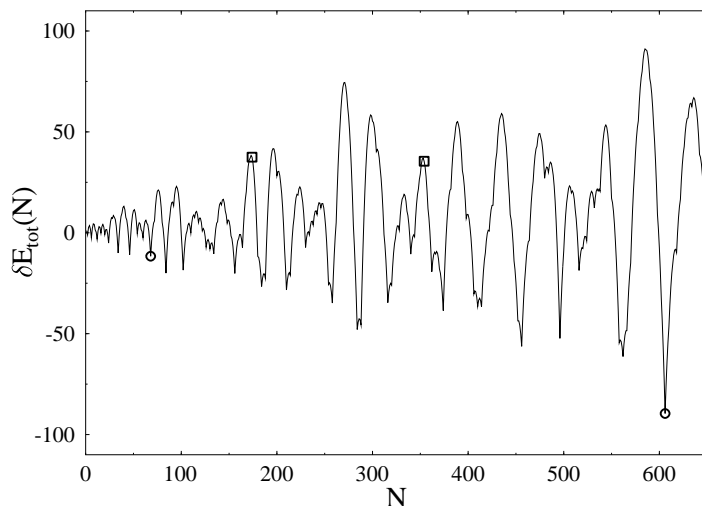


Figure 14. Shell-correction energy $\delta E_{\text{tot}}(N)$ (85) versus particle number N for the circle billiard (energy units: $E_0 = 1$). The circles mark the the closed-shell systems (at minima of δE_{tot}) with $N = 68$ and 606 , and the squares mark the mid-shell systems (near maxima of δE_{tot}) with $N = 174$ and 354 tested in figure 10.

density, for which a Gutzwiller-type trace formula [3] can be employed. $\delta E_{\text{tot}}(N)$ may, in fact, be approximated [29, 31] by either of the two following expressions

$$\delta E_{\text{tot}}(N) \simeq \int_0^\lambda (E - \lambda) \delta g(E) \mathbb{E} \simeq - \int_0^{\tilde{\lambda}} \delta \mathcal{N}(E) \mathbb{E}, \quad (87)$$

where $\delta \mathcal{N}(E) = \mathcal{N}(E) - \tilde{\mathcal{N}}(E)$ is the oscillating part of the number counting function. The two relations given in (87) are correct up to terms of order $(\lambda - \tilde{\lambda})^2$ or $[\delta \mathcal{N}(\tilde{\lambda})]^2$, respectively. The semiclassical trace formula for $\delta g(E)$ of the circular billiard is given in [10]. After its integration in (87), one obtains to leading order in \hbar the following semiclassical approximation for the shell-correction energy in terms of the POs (v, w)

$$\delta E_{\text{tot}}(N) \simeq 2 E_0^{1/4} \tilde{\lambda}^{3/4} \sum_{w=1}^{\infty} \sum_{v=2w}^{\infty} \frac{f_{v,w}}{v^2 \sqrt{\pi v \sin(w\pi/v)}} \sin \left[\frac{1}{\hbar} p_\lambda L_{v,w}^{\text{PO}} - 3v \frac{\pi}{2} + \frac{3\pi}{4} \right], \quad (88)$$

where the lengths $L_{v,w}^{\text{PO}}$ are given in (47) and $f_{v,w} = 2 - \delta_{v,2w}$.

In figure 15 we compare the semiclassical results (88) of $\delta E_{\text{tot}}(N)$ with their exact values (85) in the region $2075 \leq N \leq 2250$. We see that the agreement is best at the minima (closed main shells) and fairly good around the maxima (mid-shell systems). In regions where $\delta E_{\text{tot}}(N)$ has steep slopes, there are relatively large discrepancies, as already observed earlier [30, 31]. The reason lies in the fact that in these regions, the stair-case functions $\lambda(N)$ and $\mathcal{N}(E)$ have their largest deviations from the smooth functions $\tilde{\lambda}(N)$ and $\tilde{\mathcal{N}}(E)$, so that the missing terms of order $(\lambda - \tilde{\lambda})^2$ or $[\delta \mathcal{N}(\tilde{\lambda})]^2$ are largest, while these are smallest at closed main shells and near mid-shell regions. This is illustrated in figure 16, where we show the two curves $\mathcal{N}(E)$ and $\tilde{\mathcal{N}}(E)$ versus energy E in an interval covering the central part of the region of particle numbers shown in figure 15. They are seen to intersect at closed shells (circles) and in the mid-shell region

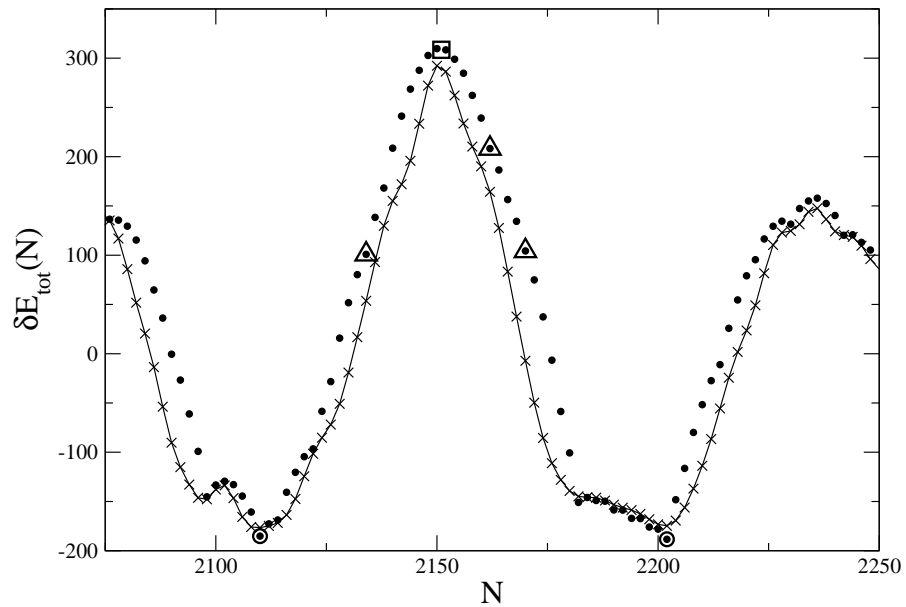


Figure 15. The same as figure 14 in a different region of particle numbers N . *Dots*: exact values (85), *crosses connected by the solid line*: semiclassical values (88). The circles mark closed-shell systems, the square marks mid-shell systems, and the triangles mark some intermediate systems tested in figure 17 below.

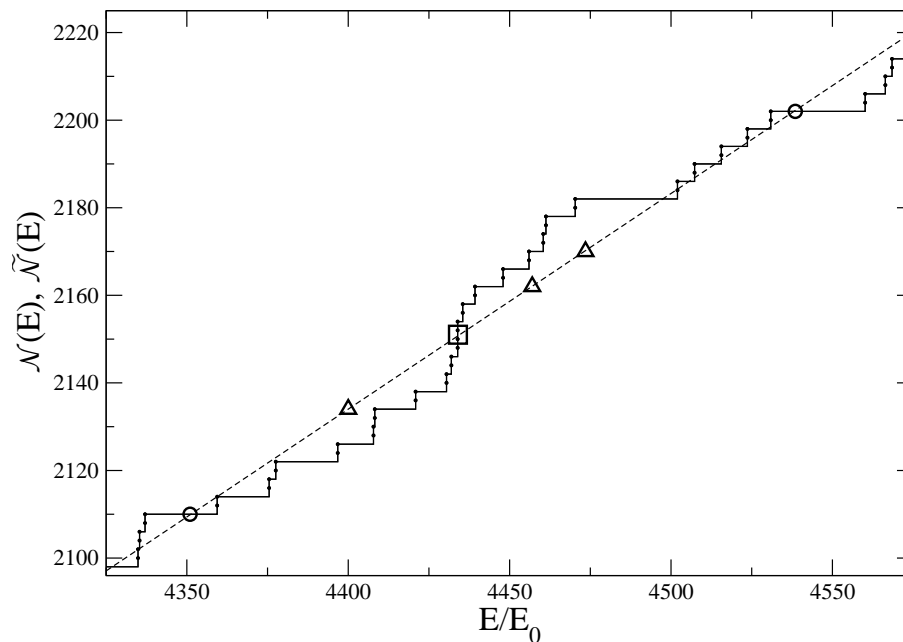


Figure 16. Number counting functions $\mathcal{N}(E)$ (*dots connected by the solid line*) and $\tilde{\mathcal{N}}(E)$ (*dashed line*). The circles, triangles and the square correspond to those in figure 15 in the region $2098 \leq N \leq 2222$.

(square). The triangles mark “difficult systems” for which the errors in the semiclassical results are largest, as seen in figure 15. There is a clear correlation between these errors and the magnitude of $\delta\mathcal{N}(E)$.

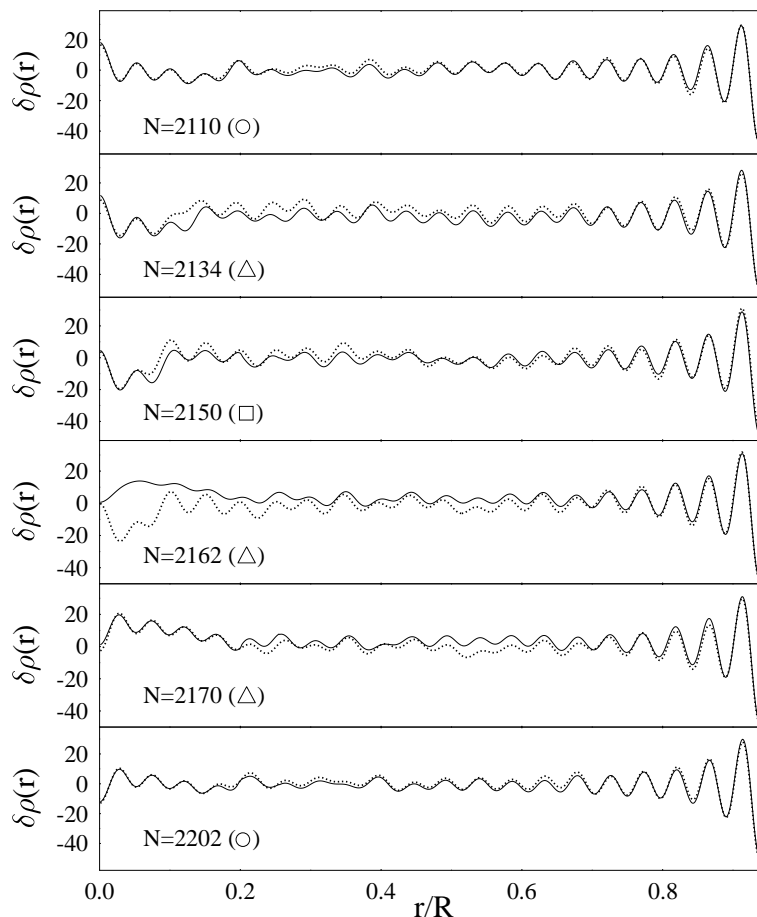


Figure 17. Oscillating part $\delta\rho(r)$ of the spatial density, obtained like in the top panels of figures 11 and 12, here for the six particle numbers marked by the circles, triangles and the square in figure 16.

We observe a similar trend for the quality of our semiclassical approximation to the spatial density oscillations. The four systems shown in figure 10, where the agreement with the quantum results is best, correspond to closed-shell and mid-shell systems (see the triangles in figure 14). In figure 17 we show the corresponding results for the five systems marked by circles, triangles and the square in figure 16. Clearly, the best agreement is reached for the closed-shell systems (circles). The correlation of the errors in $\delta\rho(r)$ with the magnitudes of $\delta\mathcal{N}(E)$ is less direct than for the shell-correction energy, but the agreement in figure 17 is clearly worst in the systems (marked by triangles) for which $\delta E_{\text{tot}}(N)$ has its steepest slope. The mid-shell system $N = 2150$ here has slightly larger errors (like also for δE_{tot} in figure 15) than those shown in the middle panels of figure 10. The same trends are also found for the kinetic energy densities.

In conclusion we can state that, with a small number of included classical orbits and straight-forward uniform approximations, the semiclassical approximation for the spatial density oscillations in the circular billiard is excellent for closed-shell systems, good for mid-shell systems and still quite satisfactory for most intermediate systems.

6. Summary

We have presented a complete classification of the closed periodic and non-periodic classical orbits in the two-dimensional circular billiard with radius R . We have divided the orbits into two classes: linear orbits, librating in the radial directions, and non-linear orbits. Analytical formulae are given for their actions, stability determinants, momentum mismatches and Morse indices. We have found that many of the orbits can undergo bifurcations at which new orbits are created. The bifurcation parameter hereby is their starting point r varied in the range $0 < r < R$. Periodic orbits can be created from non-periodic ones, and *vice versa*, in isochronous pitchfork bifurcations. Pairs of non-periodic orbits can also be generated from tangent bifurcations. Finally, a class of non-periodic orbits is generated from the linear periodic orbit upon breaking its rotational $U(1)$ symmetry by varying its starting point from $r = 0$ to $r > 0$.

Employing a recently developed closed-orbit theory [1, 2], we have investigated the semiclassical approximation of spatial density oscillations for N non-interacting fermions bound in the circular billiard in terms of its closed orbits. At the critical points (symmetry breaking at $r = 0$, bifurcation points, and the boundary $r = R$), uniform approximations have to be used in order to regularize their semiclassical amplitudes. For the symmetry breaking and both two types of bifurcations, standard uniform approximations from perturbation and bifurcation theory could be implemented in a straightforward manner, having ascertained that the bifurcations are exactly of the types known for periodic orbits as functions of other bifurcation parameters (such as energy, deformation or external field strength). Following the general analysis in [1, 2], we have demonstrated that also in the present system the linear orbits are responsible for the short-ranged regular oscillations in both particle and kinetic-energy densities, while the non-linear orbits create their long-ranged irregular oscillations. We have also confirmed here that the radial orbit with one reflection at the nearest turning point creates the Friedel oscillations near the boundary.

We have finally tested the semiclassical approximation by comparing its results to exact quantum-mechanical densities. We investigated the convergence of the sum over closed orbits and the correlations of its results with the shell structure in the total energy. We find that, using a relatively small number of included classical orbits and easy analytical uniform approximations, the semiclassical approximation is excellent for closed-shell systems, good for mid-shell systems and still quite satisfactory for most intermediate systems. This is found to hold even for moderate particle numbers $N \gtrsim 50$, in spite of the fact that *a priori* the semiclassical limit of a small Planck constant \hbar corresponds to the limit of large particle numbers.

Acknowledgments

We acknowledge stimulating discussions with A G Magner and M Gutiérrez.

Appendix. Explicit results for specific nonlinear NPOs

All the properties of the NPOs used in the semiclassical expressions (14) – (16) for the density oscillations have been given in the general analytical expressions in section 3.3 in terms of the angles α and β related by (31) and shown in figure 1. In practice, however, we need them as functions of the radial variable r . Unfortunately, for the nonlinear NPOs the inversion of the relation (32) is not possible in general; using the standard relations of the trigonometric functions this would require to find the roots of Chebychev polynomials. In the following, we give explicit results as functions of r for some simple orbits, for which the explicit inversion of (32) is possible. Some of these results have been used in examples given in the main part of the paper.

We recall that the properties of the linear NPOs are given explicitly in section 3.5; the general formulae for the Morse indices of the nonlinear NPOs are given in the systematics of section 3.6.

Appendix A.1. $v = 2, w = 1$: the triangle orbit ∇ (2,1)

For this orbit, which exists at all starting points $0 < r \leq R$ (see figure 8 for its shape), the relation (32) becomes

$$r(\alpha) = R \frac{\sin \alpha}{\cos(2\alpha)} = R \frac{x}{(1 - 2x^2)}, \quad x = \sin \alpha. \quad (\text{A.1})$$

Inverting the above we get

$$x(r) = \frac{\sqrt{R^2 + 8r^2} - R}{4r}, \quad \alpha(r) = \arcsin \left(\frac{\sqrt{R^2 + 8r^2} - R}{4r} \right). \quad (\text{A.2})$$

The length of the ∇ orbit becomes

$$L_{2,1}(r) = 4R \frac{\cos^3 \alpha}{\cos(2\alpha)} = 4R \frac{(1 - x^2)^{3/2}}{(1 - 2x^2)}, \quad (\text{A.3})$$

and the Jacobian becomes

$$\mathcal{J}_{2,1}(r) = \frac{R}{p_\lambda} \tan(2\alpha) \left[\sin \alpha + \frac{r}{R} (1 + 6 \sin^2 \alpha) \right]. \quad (\text{A.4})$$

Inserting $\alpha(r)$ from (A.2) into (A.3) and (A.4), both quantities are obtained explicitly as functions of r . For small r we get the Taylor expansions

$$L_{2,1}(r) = 4R + 2 \frac{r^2}{R} + \mathcal{O} \left(\frac{r}{R} \right)^4, \quad \mathcal{J}_{2,1}(r) = 4 \frac{R}{p_\lambda} \left(\frac{r}{R} \right)^2 + \mathcal{O} \left(\frac{r}{R} \right)^4. \quad (\text{A.5})$$

Appendix A.2. $v = 3, w = 1$: the orbit Λ (3,1)

This orbit exists only for $r \geq r_1 = R/3$, where it bifurcates from the linear orbit $L_+^{(1)}$. At $r = r_{3,1}^{\text{PO}} = R/2$ the triangular PO Δ (3,1) bifurcates from it (see the bifurcation scenarios in the left panels of figure 2 and the shapes of the orbit in figure 3). At

the boundary $r = R$ it becomes identical with the squared PO \square (4,1). The relation between r and α is given by

$$r(\alpha) = R \frac{\sin \alpha}{\sin(3\alpha)} = R \frac{1}{(3 - 4x^2)}. \quad (\text{A.6})$$

Inverting the above, we get

$$\sin \alpha(r) = x(r) = \frac{1}{2} \sqrt{3 - \frac{R}{r}}, \quad r \geq r_1 = R/3. \quad (\text{A.7})$$

The explicit expressions for its length, momentum mismatch and Jacobian are

$$L_{3,1}(r) = 2\sqrt{\frac{R+r}{r}}(R+r), \quad (\text{A.8})$$

$$Q_{3,1}(r) = \frac{R^2}{2r^3}(3r-R) - 1, \quad (\text{A.9})$$

$$\mathcal{J}_{3,1}(r) = \frac{2}{Rp_\lambda}(2r-R)(3r-R)\sqrt{\frac{r+R}{r}}. \quad (\text{A.10})$$

Note that, although the relations (A.6) and (A.7) only hold for $r \geq r_1$, the three functions (A.8) – (A.10) can be continued analytically to $r < r_1$ and are real in the entire interval $0 \leq r \leq R$. For $r < r_1$, we can consider them as the (real) properties of an imaginary “ghost orbit”; they are required in the uniform approximation (78) for the pitchfork bifurcation at r_1 discussed in section 4.2.1.

Appendix A.3. $v = 4, w = 1$: the “pentagon” orbits P (4,1) and P’ (4,1)’

This pair of NPOs is created in a tangent bifurcation at

$$r_{4,1} = 0.682489R. \quad (\text{A.11})$$

Some of their shapes are shown in figure 4, and their bifurcation scenario is shown in the right panels of figure 2. At the boundary $r = R$, P becomes identical to the pentagonal (not self-crossing) PO (5,1), and P’ becomes identical to the triangular PO Δ (3,1). The connection between r and α of this orbit is given by

$$r(\alpha) = -R \frac{\sin \alpha}{\cos(4\alpha)} = -R \frac{x}{(1 - 8x^2 + 8x^4)}. \quad (\text{A.12})$$

The inversion of $r(x)$ leads to a fourth-order algebraic equation whose analytic solution is possible but cumbersome. Without writing it down explicitly, we can make the following statements. The real solutions for $x(r)$ consist of two branches starting from the minimum value of $r(x)$ which is found at $x_0 = [(2 + \sqrt{10})/12]^{1/2} = 0.655889$ and has the value $r(x_0) = r_{4,1}$ given in (A.11). The two branches correspond to the two orbits P and P’ born in a tangent bifurcation at $r_{4,1}$. The orbit P’ corresponds to the lower branch with $x'_1 = 1/2 \leq x \leq x_0$. The orbit P corresponds to the upper branch with $x_0 \leq x \leq x_1 = \sin(3\pi/10) = 0.809017$. At $r_{4,1}^{\text{PO}} = R/\sqrt{2}$ it undergoes a pitchfork bifurcation, whereby the squared PO \square (4,1) is born. The lengths, momentum mismatches and Jacobians can in principle be evaluated explicitly but are most easily calculated numerically using the general formulae given in section 3.3. We note that the

analytical continuation to $r < r_{4,1}$, where the orbits are imaginary “ghost orbits”, here leads to complex quantities, which is a characteristic of the tangent bifurcation [16].

For the sake of an illustration, we give in the following the results for the similar pair of NPOs with $(v, w) = (5, 1)$, for which the two branches of $x(r)$ can be given explicitly.

Appendix A.4. $v = 5, w = 1$: the pair of orbits $(5, 1)$ and $(5, 1)'$

These orbits are born in a tangent bifurcation at the point $r_{5,2} = 4R/5$. Inverting

$$r(\alpha) = -R \frac{\sin \alpha}{\sin(5\alpha)} = \frac{-R}{(5 - 20x^2 + 16x^4)}, \quad (\text{A.13})$$

which has a minimum at $x_0 = \sqrt{5/8}$, yields a bi-quadratic equation with the simple solutions

$$\sin \alpha(r) = x(r) = \frac{1}{2} \sqrt{\frac{1}{2}(5 \pm \sqrt{5 - 4R/r})}, \quad (\text{A.14})$$

whereby the two signs correspond to the two orbits. Their properties are

$$L_{5,1}(r) = R \sqrt{\frac{1}{2}(3 \mp \sqrt{5 - 4R/r})} \left(4 + \frac{r}{R} \pm \frac{r}{R} \sqrt{5 - 4R/r} \right), \quad (\text{A.15})$$

$$Q_{5,1}(r) = -1 + \frac{R^2}{4r^2} \left(5 \mp \sqrt{5 - 4R/r} \right), \quad (\text{A.16})$$

$$\begin{aligned} \mathcal{J}_{5,1}(r) &= \frac{1}{Rp_\lambda} \sqrt{\frac{1}{2}(3 \mp \sqrt{5 - 4R/r})} \\ &\times \left[4R^2 + 30r^2 - 29Rr \pm r(-9R + 10r)\sqrt{5 - 4R/r} \right]. \end{aligned} \quad (\text{A.17})$$

The upper and lower signs in the above expressions correspond to the orbits $(5, 1)$ and $(5, 1)'$, respectively. At $r_{5,1}^{\text{PO}} = R \cos(\pi/5)$, which is a zero of the term in square brackets on the second line in (A.17) (taken with the upper sign), the NPO $(5, 1)$ gives birth to the regular pentagon PO $(5, 1)$ in a pitchfork bifurcation.

References

- [1] Roccia J and Brack M 2008 *Phys. Rev. Lett.* **100** 200408
- [2] Roccia J, Brack M, Koch A and Murthy M V N 2009 *Preprint* arXiv:0903.2172v1 [math-ph]
- [3] Gutzwiller M C 1967 *J. Math. Phys.* **8** 1979, and earlier references quoted therein
Gutzwiller M C 1990 *Chaos in classical and quantum mechanics* (New York: Springer-Verlag)
- [4] Brack M and Bhaduri R K 2003 *Semiclassical Physics*, Frontiers in Physics, Vol 96, revised edition (Bolder, USA: Westview Press)
- [5] Brack M and Murthy M V N 2003 *J. Phys. A: Math. Gen.* **36** 1111
- [6] Robinett R W 1996 *Am. J. Phys.* **64** 440
- [7] Baltus H P and Hilf E R 1976 *Spectra of Finite Systems* (Mannheim: Bibliographisches Institut)
- [8] Berry M V and Howls C J 1994 *Proc. R. Soc. Lond. A* **447** 527
- [9] Balian R and Bloch C 1972 *Ann. Phys. (N. Y.)* **69** 76
- [10] Reimann S M, Brack M, Magner A G, Blaschke J and Murthy M V N 1996 *Phys. Rev. A* **53** 39
- [11] Lin W A and Jensen R V 1997 *Phys. Rev. E* **56** 5251
- [12] Ozorio de Almeida A M and Hannay J H 1987 *J. Phys. A: Math. Gen.* **20** 5873
- [13] Tomsovic S, Grinberg M and Ullmo D 1995 *Phys. Rev. Lett.* **75** 4346
Ullmo D, Grinberg M and Tomsovic S 1996 *Phys. Rev. E* **54** 135
- [14] Sieber M 1996 *J. Phys. A: Math. Gen.* **29** 4715
- [15] Creagh S C 1996 *Ann. Phys. (N. Y.)* **248** 60
- [16] Schomerus H and Sieber M 1997 *J. Phys. A: Math. Gen.* **30** 4537
- [17] Sieber M and Schomerus H 1998 *J. Phys. A: Math. Gen.* **31** 165
- [18] Brack M and Tanaka K 2008 *Phys. Rev. E* **77** 046205
- [19] Brack M, Meier P and Tanaka K 1999 *J. Phys. A: Math. Gen.* **32** 331
- [20] Ozorio de Almeida A M 1988 *Hamiltonian Systems: Chaos and Quantization* (Cambridge: Cambridge University Press)
- [21] Abramowitz M and Stegun I A 1972 *Handbook of Mathematical Functions*, 9th printing (New York: Dover)
- [22] Meyer K R 1970 *Trans. Amer. Math. Soc.* **149** 95
- [23] Jänich K 2007 *Mathematical remarks on transcritical bifurcations in Hamiltonian systems Preprint* arXiv:0710.3464v1 [math:SG]
- [24] Then H L 1999 *Diploma thesis* (Universität Ulm)
- [25] Brack M, Mehta M and Tanaka K 2001 *J. Phys. A* **34** 8199
- [26] Main J and Wunner G 1997 *Phys. Rev. A* **55** 1743
- [27] Schomerus H 1998 *J. Phys. A: Math. Gen.* **31** 4167
- [28] Agam O 1996 *Phys. Rev. B* **54** 2607
- [29] Strutinsky V M 1975 *Nukleonika (Poland)* **20** 679
Strutinsky V M and Magner A G 1976 *Sov. J. Part. Nucl.* **7** 138
- [30] Meier P, Brack M and Creagh S C 1997 *Z. Phys. D* **41** 281
- [31] Leboeuf P and Monastera A G 2003 *Nucl. Phys. A* **724** 69
Leboeuf P 2005 *Lecture Notes in Physics* **652** 245
Roccia J and Leboeuf P 2007 *Phys. Rev. C* **76** 014301
- [32] Strutinsky V M 1966 *Sov. J. Nucl. Phys.* **3** 449
Strutinsky V M 1967 *Nucl. Phys. A* **95** 420
- [33] Brack M, Damgård J, Jensen A S, Pauli H C, Strutinsky V M and Wong C Y 1972 *Rev. Mod. Phys.* **44** 320